

1 Atmospheric H₂ observations from the NOAA Cooperative 2 Global Air Sampling Network

3 Gabrielle Pétron^{1,2}, Andrew M. Crotwell^{1,2}, John Mund^{1,2}, Molly Crotwell^{1,2}, Thomas Mefford^{1,2},
4 Kirk Thoning², Bradley Hall², Duane Kitzis^{1,2}, Monica Madronich^{1,2}, Eric Moglia^{1,2}, Donald
5 Neff^{1,2}, Sonja Wolter^{1,2}, Armin Jordan³, Paul Krummel⁴, Ray Langenfelds⁴, John Patterson⁵
6 *Correspondence to:* Gabrielle Pétron (gabrielle.petron@noaa.gov)

7

8 1. Cooperative Institute for Research in Environmental Sciences, CU Boulder, USA

9 2. NOAA Global Monitoring Laboratory, Boulder, USA

10 3. Max-Planck-Institute for Biogeochemistry (MPI-BGC), Jena, Germany

11 4. Commonwealth Scientific and Industrial Research Organisation - Environment, Aspendale, Australia

12 5. Department of Earth System Science, University of California, Irvine, USA

13

14

15 **Abstract.** The NOAA Global Monitoring Laboratory (GML) measures atmospheric hydrogen (H₂) in
16 grab-samples collected weekly as flask pairs at over 50 sites in the Cooperative Global Air Sampling
17 Network. Measurements representative of background air sampling show higher H₂ in recent years at all
18 latitudes. The marine boundary layer (MBL) global mean H₂ was 552.8 ppb in 2021, 20.2 ± 0.2 ppb higher
19 compared to 2010. A 10 ppb or more increase over the 2010-2021 average annual cycle was detected in
20 2016 for MBL zonal means in the tropics and in the Southern Hemisphere. Carbon monoxide
21 measurements in the same air samples suggest large biomass burning events in different regions likely
22 contributed to the observed interannual variability at different latitudes. The NOAA H₂ measurements
23 from 2009 to 2021 are now based on the World Meteorological Organization Global Atmospheric Watch
24 (WMO GAW) H₂ mole fraction calibration scale, developed and maintained by the Max-Planck Institute
25 for Biogeochemistry (MPI-BGC), Jena, Germany. GML maintains eight H₂ primary calibration standards
26 to propagate the WMO scale. These are gravimetric hydrogen-in-air mixtures in electropolished stainless
27 steel cylinders (Essex Industries, St. Louis, MO), which are stable for H₂. These mixtures were calibrated
28 at the MPI-BGC, the WMO Central Calibration Laboratory (CCL) for H₂, in late 2020 and span the range
29 250-700 ppb. We have used the CCL assignments to propagate the WMO H₂ calibration scale to NOAA
30 air measurements performed using Gas Chromatography-Helium Pulse Discharge Detector instruments
31 since 2009. To propagate the scale, NOAA uses a hierarchy of secondary and tertiary standards, which
32 consist of high-pressure whole air mixtures in aluminum cylinders, calibrated against the primary and
33 secondary standards respectively. Hydrogen at the ppb-level has a tendency to increase in aluminum
34 cylinders over time. We fit the calibration histories of these standards with 0-2nd order polynomial
35 functions of time and use the time-dependent mole fraction assignments on the WMO scale to reprocess
36 all tank air and flask air H₂ measurement records. The robustness of the scale propagation over multiple
37 years is evaluated with the regular analysis of target air cylinders and with long-term same air
38 measurement comparison efforts with WMO GAW partner laboratories. Long-term calibrated, globally
39 distributed and freely accessible measurements of H₂ and other gases and isotopes continue to be essential
40 to track and interpret regional and global changes in the atmosphere composition. The adoption of the
41 WMO H₂ calibration scale and subsequent reprocessing of NOAA atmospheric data constitute a
42 significant improvement in the NOAA H₂ measurement records.

43

44 1 Introduction

45

46 High quality and sustained observations are essential to track and study changes in atmospheric trace gas
47 distributions. Ambient air measurement programs for trace gases provide objective data to track air
48 pollution levels [Oltmans and Levy, 1994; Thomson et al., 2004; Tørseth et al., 2012; Schultz et al., 2015;
49 Cooper et al., 2020; WMO, 2022], to study how a mix of sources (and sinks) impact the air composition
50 [Ciais et al., 1995; Pétron et al., 2012; Langenfelds et al., 2002; Brito et al., 2015] and to constrain and
51 evaluate fluxes and their trends at scales of interest [von Schneidemesser et al., 2010; Simpson et al.,
52 2012; Propper et al., 2015; Montzka et al., 2018; Friedlingstein, 2022; Heiskanen et al., 2022; Storm et
53 al., 2023].

54

55 H₂ is a trace gas in the Earth's atmosphere and its abundance can indirectly impact climate and air quality.
56 The analysis of H₂ measurements in firm air collected in Antarctica reveal that H₂ levels in the
57 high-latitude southern hemisphere grew by some 70% (330 to 550 ppb, 1 ppb = 1 mole of gas per billion
58 (10⁹) moles of air) over the 20th century [Patterson et al., 2021; 2023]. Greenland firm air covers less
59 depth and time but results are consistent with a 30% increase in high-latitude northern hemisphere H₂
60 from 1950 to the late 1980s [Patterson et al., 2023]. Growing emissions related to fossil fuel burning most
61 likely were behind this rise in H₂ [Patterson et al., 2021]. Results also show that H₂ in both polar regions
62 leveled off after the 1990s [Patterson et al., 2021, 2023].

63

64 H₂ has been viewed as a potential low or zero carbon energy carrier for close to five decades [Yap and
65 McLellan, 2023]. Since 2020 there has been renewed interest in the hydrogen economy [Yap and
66 McLellan, 2023] spurred by a rise in announcements of public and private projects to produce low carbon
67 H₂, also referred to as “blue” H₂ produced from natural gas with carbon capture, utilization and storage, or
68 “green” H₂ produced using renewable energy [Hydrogen Council and McKinsey & Company, 2023]. In
69 2021, H₂ global demand was over 94 million tonnes or 2.5 % of global final energy consumption [IEA,
70 2022]. This demand was almost entirely driven by refineries and a few industries (ammonia, methanol
71 and steel) and H₂ production almost entirely relied on fossil fuels with unabated emissions (“gray H₂”,
72 [IEA, 2022]). As of December 2023, over 1,400 announced projects globally (worth US\$ 570 billion) are
73 anticipated to increase the global H₂ production capacity by 45 million tonnes through 2030 [Hydrogen
74 Council and McKinsey & Company, 2023].

75

76 Studies of the potential short-term and long-term climate impacts of increased H₂ production and use have
77 called for more research to better understand the current and future H₂ supply chain and end-use
78 emissions of H₂ and GHGs [Ocko and Hamburg, 2022; Longden et al., 2022; de Kleijne et al., 2022;
79 Bertagni et al., 2022; Warwick et al., 2023]. Global, high quality and sustained atmospheric
80 measurements of H₂ can provide independent information to document its distribution and study its
81 sources and sinks and how they may change.

82

83 The National Oceanic and Atmospheric Administration (NOAA) Cooperative Global Air Sampling
84 Network comprises over 50 surface and mostly remote sites (<https://gml.noaa.gov/ccgg/flask.html>). At
85 each site and on a weekly basis, local partners collect air in two 2.5-L glass flasks, and then return the
86 flasks to the NOAA Global Monitoring Laboratory (GML) in Boulder, Colorado, USA, for measurements
87 of major long-lived greenhouse gases, carbon dioxide (CO₂), methane (CH₄), nitrous oxide (N₂O), sulfur

88 hexafluoride (SF₆), as well as carbon monoxide (CO) and hydrogen (H₂) [Conway et al., 1994; Novelli et
89 al., 1999; Dlugokencky et al., 2009]. The network is a contributor to the World Meteorological
90 Organization (WMO) Global Atmospheric Watch (GAW) Programme, which promotes and coordinates
91 international scientific efforts and free access to long-term atmospheric observations [WMO, 2022].

92

93 CO and H₂ are important trace gases that share sources with CO₂ and CH₄ (fossil fuel burning, biofuel
94 burning and wildfires). Reaction with hydroxyl radicals (OH) is the main sink for CH₄ and CO and an
95 important sink for H₂. Both H₂ and CO are also produced during the chemical oxidation of CH₄ and
96 nonmethane hydrocarbons. Soil uptake by bacteria accounts for 75% of the total H₂ sink. H₂ and CO have
97 much shorter atmospheric lifetimes than CO₂ and CH₄: 2-3 months for CO and close to 2 years for H₂.
98 The H₂ global mean atmospheric lifetime is largely driven by the soil sink strength. The H₂ lifetime
99 related to the oxidation by OH is estimated to be 8-9 years [Price et al., 2007; Warwick et al., 2022].

100

101 Novelli et al. [1991, 1992] reported for NOAA on testing the air sampling approach (flask type, stopcock
102 fitting, wet/dry air, untaped versus taped glass flasks to minimize direct sunlight exposure) and an
103 analytical instrument consisting of a gas chromatograph (GC) and a reduction gas analyzer (RGA, from
104 Trace Analytical Inc., California) that could measure both CO and H₂. Around that time, other
105 laboratories had also adopted the technique for CO and H₂ measurements in discrete air samples or in situ.
106 Khalil and Rasmussen [1989, 1990] reported on H₂ measurements of whole air samples collected weekly
107 in triplicate electropolished stainless steel flasks between October 1985 and April 1989 at the four NOAA
108 atmospheric baseline observatories (Point Barrow, Mauna Loa, Samoa, South Pole), Cape Mearns,
109 Oregon, Cape Kumukahi, Hawaii and at the Kennaook/Cape Grim Observatory, Tasmania. These
110 measurements showed that, contrary to CO₂, CH₄, N₂O and CO, background air H₂ levels were higher in
111 the Southern Hemisphere (SH) than in the Northern Hemisphere (NH). 1985-1987 monthly mean
112 observed H₂ ranged between 500-520 ppb at the South Pole and between 455 and 520 ppb at Point
113 Barrow. H₂ exhibited a strong seasonal cycle at extratropical latitudes especially in the NH and the
114 seasonal cycles in both hemispheres were offset by 1-2 months only.

115

116 In 1995, H₂ mole fraction calibration standards were prepared gravimetrically in aluminum cylinders
117 (Scott Marrin Inc., Riverside, CA) and five of them (spanning 485-603 ppb) were used to define the
118 NOAA H₂ X1996 calibration scale. Working standards used in the NOAA flask analysis laboratory
119 between 1988 and 1996 were reassigned H₂ mole fractions and flask air measurements were reprocessed
120 to be on the X1996 scale. Novelli et al. [1999] described the early NOAA H₂ measurements and reported
121 H₂ time series starting in the late 1980s or early 1990s (depending on the site) for 50 sites in the NOAA
122 Cooperative Global Air Sampling Network.

123

124 Simmonds et al. [2000] reported in-situ high-frequency GC-RGA3 measurements of H₂ at the Mace Head
125 baseline atmospheric monitoring station on the Atlantic coast of Ireland for the 1994-1998 period. They
126 found that the background air at Mace Head had lower monthly mean H₂ (470-520 ppb) than background
127 air masses measured at the Kennaook/Cape Grim observatory (510-530 ppb) from July to April. Some of
128 the 40 min H₂ observations showed 10-200 ppb short-term H₂ enhancements above baseline levels. The
129 authors derived an estimate of European emissions with an inverse model of enhanced H₂ in air masses
130 impacted by upwind sources of pollution. They also observed that nighttime measurements in low wind

131 conditions reflected local depletion of H₂. The authors derived variable mean deposition velocities and
132 found that the H₂ soil sink was likely a process that occurred year-round in the area.

133

134 After 1996 and until 2008, the NOAA H₂ measurement program used successive working standards that
135 were assigned based on GC-RGA measurements against the previous standards. With hindsight, the
136 NOAA X1996 calibration scale transfer and the early NOAA H₂ measurements had several limitations
137 which are briefly described below and in more detail in the Supplementary Information section S1.

138

139 By the late 1990s, same air or colocated air sample measurement comparison between NOAA and the
140 Commonwealth Scientific and Industrial Research Organisation (CSIRO) for the Kennaook/Cape Grim
141 Observatory and Alert, Canada, flask air analyses showed an increasing bias for H₂ between the two
142 laboratories [Masarie et al., 2001; Francey et al., 2003]. Further laboratory tests by several WMO/GAW
143 measurement laboratories revealed the RGA detector response was non linear and required frequent
144 calibration. Additionally measurement laboratories found that the H₂ mole fraction for air standards,
145 especially those stored in high pressure aluminum cylinders, could drift at rates of a few parts per billion
146 (ppb) to tens of ppb per year [Novelli et al., 1999; Masarie et al., 2001; Jordan and Steinberg, 2011].

147

148 To address these compounding issues, in 2008 NOAA GML tested a new analytical instrument: a gas
149 chromatograph with a pulse discharge helium ionization detector (GC-HePDD) [Wentworth et al., 1994].
150 The technique showed very good performance with a stable and linear response over the 0-2000 ppb
151 range and it was adopted for the calibration scale propagation and flask air analysis of H₂ in 2009 [Novelli
152 et al., 2009]. Around that time GML also began testing electropolished stainless steel cylinders (Essex
153 Industries, St. Louis, MO) filled with dry air for stability.

154

155 In 2007-2008, GML prepared six new gravimetric air mixtures in electropolished stainless steel cylinders
156 spanning 250-600 ppb H₂. At that time, the new gravimetric mixtures differed by about +20 ppb
157 compared to two H₂ secondary standards values assigned on the NOAA H₂ X1996 scale. For the next
158 decade, GML kept using the NOAA X1996 calibration scale while also conducting routine measurements
159 of the H₂ secondary standards against the 2007/2008 gravimetric mixtures.

160

161 The GC-HePDD H₂ measurements on the NOAA H₂ X1996 scale remained biased compared to GAW
162 partner measurements and the NOAA H₂ data from the global network flasks were not released publicly
163 after 2005. SI sections S1-3 and SI Table 1 provide additional information on issues impacting the
164 1988-2008 NOAA H₂ measurements on RGAs, and related information from the CSIRO and Max-Planck
165 Institute for Biogeochemistry (MPI-BGC) H₂ measurement programs. The more precise and better
166 calibrated NOAA H₂ measurement records date back to 2009/2010 and are the main focus of this paper.

167

168 In Fall 2020, GML initiated an effort to 1) adopt the WMO MPI X2009 H₂ calibration scale [Jordan and
169 Steinberg, 2011] for future measurements and 2) convert GML H₂ measurements made on GC-HePDD
170 instruments (beginning in late 2009) to that scale. This paper describes the MPI X2009 H₂ calibration
171 scale propagation within GML and the revised measurements from the NOAA Cooperative Global Air
172 Sampling Network flask air samples analyzed since late 2009. We show very good agreement for the
173 reprocessed NOAA H₂ data for different WMO GAW measurement comparison efforts. The revised
174 NOAA GML flask air H₂ dry air mole fraction measurement records for over 50 surface sites from

175 2009-2021 are publicly available [Pétron et al., 2023a]. This new dataset complements other WMO GAW
176 H₂ measurement datasets and provides reliable observational constraints for the study of atmospheric H₂
177 global distribution and budget since 2009. Future NOAA H₂ dataset updates will be released as we use
178 continued calibration results to reliably track the drift in standards and revise their assignments.

179

180 **2 Adoption of the WMO MPI X2009 H₂ calibration scale**

181

182 To infer fluxes and trends from atmospheric measurements, scientists need to reliably detect small
183 temporal and spatial gradients in the abundance of trace gases. This requires comparable data across time
184 and across monitoring networks to ensure biases are minimized and do not influence interpretation. The
185 use of a common calibration scale among measurement laboratories ensures data are traceable to a
186 common reference. It is the first step in preventing biases that could stem from using different references.

187

188 In this section, we introduce the NOAA GML H₂ calibration standard hierarchy and describe the adoption
189 of the WMO MPI X2009 H₂ scale. Calibration at GML is based on a hierarchy of standards (primary,
190 secondary, tertiary) and a dedicated H₂ calibration system used to transfer the scale from the primary
191 standards to secondary and tertiary standards. An important quality assurance procedure within GML is
192 the routine measurement of dedicated quality control cylinders (referred to as "Target" tanks) to track
193 instrument performance. Results are discussed in relation to the uncertainty of the flask air analysis
194 systems and consistency of the MPI X2009 H₂ scale implementation.

195

196 **2.1 NOAA GML H₂ primary standards**

197

198 In 2007-2008, six mixtures of H₂ in dry air were prepared gravimetrically at GML in electropolished
199 stainless steel 34L cylinders ([Novelli et al., 2009], and Table 1). The highest H₂ mole fraction tank
200 developed a leak and was lost. The remaining set of five standards covered the range 250 ppb to 600 ppb
201 for H₂. Three standards in electropolished stainless steel cylinders were added in 2019 to extend the upper
202 limit of the calibration range to 700 ppb H₂ and evaluate the stability of the initial set over the intervening
203 years. In 2020, these eight standards were designated as NOAA GML's highest level H₂ standards. We
204 refer to them as the NOAA H₂ primary standards throughout this document even though they are not used
205 to independently define the scale.

206

207 The eight primary standards were analyzed by the WMO Central Calibration Laboratory (CCL) for H₂
208 hosted by the MPI-BGC in Jena, Germany, on their GC-PDD system in November 2020. The results
209 listed in Table 1 are reported on the MPI X2009 H₂ calibration scale [Jordan and Steinberg, 2011]. The
210 CCL uncertainty estimates listed in Table 1 refer to the standard deviation of the 25-32 discrete H₂
211 measurements made for each standard. Until they are recalibrated by the CCL, we add an 0.5 ppb 1-sigma
212 uncertainty to these assignments. This is the currently reported CCL reproducibility for their GC-PDD H₂
213 measurements. It accounts for potential longer term uncertainty in calibration results that would not be
214 evident in the standard deviations of measurements made close in time.

215

216 **2.2 MPI X2009 H₂ calibration scale transfer**

217

218 GML has separate, dedicated analytical systems for scale propagation and flask air analyses. Novelli et al.
219 [2009] describe the GC-HePDD instruments and the operating parameters in detail. GML has used three
220 GC-HePDD instruments so far. Each is identified by a unique internal instrument identification code: H9
221 for tank calibrations and H8 and H11 for flask analyses. The GC-HePDD instruments' responses are
222 linear (within 0.3%) up to 2000 ppb. They are configured for ppb level sensitivity and calibrated over the
223 200-700 ppb range, which is optimal for global and regional background air analysis.

224

225 The GML H₂ primary standards are used to periodically calibrate the H9 instrument response for the
226 analysis and value assignment of lower level standards. The stability and longevity of the primary
227 standards are critical to ensure the consistency of the GML H₂ measurements over long periods of time as
228 required for trend analysis.

229

230 The H₂ secondary and tertiary standards used in GML are whole air mixtures in high pressure aluminum
231 cylinders (Luxfer USA). Most were filled at the GML standard air preparation facility at the Niwot Ridge
232 mountain research station using a Rix Industries (Benicia, CA) SA6 oil-free compressor [Kitzis, 2017].
233 Two additional tertiary standards were purchased from Scott Marrin. All GML tank air mixtures have a
234 unique combination of an alphanumeric cylinder ID and a fill code letter (A-Z) tied to a fill date.

235

236 Aluminum tanks are known to be unstable for storing H₂ in air standards [Jordan and Steinberg, 2011].
237 Therefore regular analyses of standards on the tank calibration system are critical for quantifying drift to
238 allow a time dependent value assignment on the MPI X2009 H₂ calibration scale.

239

240 GML uses python software developed in-house to record calibration data, compute mole fractions, and
241 evaluate the stability of H₂ mole fractions over time. All mole fraction assignments and associated drift
242 coefficients for standards used to propagate a calibration scale are stored in a database table that can be
243 accessed by the data processing software. The software allows for 0-2nd order polynomial drift functions.
244 As new calibration results are available, the drift correction and assignment for a particular tank ID and
245 fill code are revised as needed and the affected data are reprocessed.

246

247 **2.2.1 Scale transfer: 2009-2019**

248

249 From 2007 through mid-April 2019, the H₂ tank air calibration on the H9 instrument was conducted using
250 a single standard gas (primary or secondary standard) to calibrate the "unknown" (secondary or tertiary)
251 standards. A tank calibration event consisted of alternating injections of the reference/standard gas and
252 the "unknown" tank air with typically seven or more unknown air injections. The first aliquot in a multi
253 injection measurement sequence on H9 is often slightly biased (due to subtle timing differences with the
254 regulator flush cycle) and is not used. The ratio of the H₂ peak height for each valid "unknown" air
255 injection and the mean peak height of two bracketing reference gas injections (or sometimes only one
256 preceding or following reference gas injection) is multiplied by the reference/standard gas known H₂ mole
257 fraction to calculate the "unknown" air injection mole fraction. Results for a tank air calibration event are
258 defined by the mean and the standard deviation of the calculated H₂ mole fractions for five or more
259 retained "unknown" air injections. Typically, the standard deviation for a tank air calibration event on H9
260 is less than 1 ppb.

261

262 Prior to the 2023 GML H₂ data reprocessing, GML used peak area for the GC-HePDD as described in
263 Novelli et al. [1999]. However, we saw that for some Helium carrier gas tanks (Airgas Ultra High Purity,
264 99.999% purity), the H₂ chromatogram peak had a tail or a noisy baseline. Since the H₂ peak height was
265 less affected, we use peak height ratios for all GC-HePDD measurements. In 2023, GML switched to
266 Matheson Research Grade Helium carrier gas for the GC-HePDDs (99.9999% purity).

267

268 The calibration results for the two H₂ secondary standards used between 2009 and April 2019 are plotted
269 in Figure 1 and final assignments are listed in SI Table 2. A small non zero y-intercept for H9 (see next
270 section) likely explains the biased results for CC119811 against the lowest primary standards (SX-3558
271 and SX-3543). Results against SX-3558 were not used for value assigning either secondary standards and
272 results against SX-3543 were not used for CC119811.

273

274 CA03233 was stable for H₂ over its time of use and has an assignment of 502.8 ppb H₂. H₂ in CC119811
275 exhibited a small linear drift and its value assignment is time dependent with a growth rate of 2 ppb/yr.
276 Between 2009 and 2019, these two secondary standards were used on H9 to calibrate seventeen H₂
277 tertiary standards used in the NOAA flask analysis laboratory.

278

279 **2.2.2 Scale transfer: 2019-present**

280

281 Beginning in April 2019, GML transitioned H9 to use a multi-point calibration strategy to better define
282 the instrument response. The eight H₂ primary standards are measured relative to a reference air tank
283 (CC49559, filled with ambient Niwot Ridge dried air) to calibrate the instrument response. A
284 multi-standard response calibration episode for H9 involves the alternating injections from the reference
285 air tank and each primary standard. Each standard is injected 8 times alternating with reference air
286 aliquots. The entire response calibration sequence takes close to 15 hours. GML has performed an H9
287 instrument response calibration 2 to 3 times a year, followed by tank calibrations over a 10-14 day period
288 each time.

289

290 The H9 instrument response function is calculated as the best linear fit to the primary standards' mean
291 normalized chromatogram peak heights and their CCL H₂ mole fraction assignments. H9 calibration
292 curves are assumed to be valid for several weeks during which time other air cylinders are analyzed
293 relative to the same reference tank.

294

295 Between April 2019 and December 2022, the H9 instrument response was determined relative to the
296 primary standards nine times. Figure 2a shows the deviations of the H9 linear response functions from the
297 line defined by computing the mean value for the intercept and slope of the 2019-2022 response
298 functions. The instrument response has remained stable within +/- 1 ppb over this time period over the
299 range 200-700 ppb. The residuals to each linear fit over this time period are all within the -0.6 ppb to 0.5
300 ppb range (Figure 2b). The linear fit y-intercept ranges between 3.9 and 5.5 ppb (not shown). Prior to
301 2019, we assumed a zero intercept for the H9 one point calibration. If we assume a y-intercept around 5
302 ppb was more likely, it is possible the pre-2019 H9 measurements (with 1 point calibration) were biased
303 by ~1% of the difference between the tank air and the standard H₂ mole fractions. We do not correct for
304 this potential bias at this time.

305

306 Since April 2019, a tank air measurement sequence on H9 has consisted of 7 tank air injections, each
307 bracketed by reference air injections. The peak heights for the first injections of reference air and tank air
308 can have a small low bias and are not used. The normalized peak heights for the valid tank air injections
309 are converted to H₂ mole fractions using the most recent H9 response function. The average and standard
310 deviation of the retained injection H₂ mole fractions are stored in a database table.

311

312 **2.2.3 H₂ standards and calibration approach for the flask air analysis system**

313

314 H₂ in flask air samples is measured in addition to long-lived GHGs (CO₂, CH₄, N₂O, SF₆) and CO by the
315 Measurement of Atmospheric Gases that Influence Climate Change (MAGICC) system in the NOAA
316 GML Boulder laboratory. Until mid 2019, GML operated two nearly-identical automated flask air
317 analytical systems: MAGICC-1 (1997-2019) and MAGICC-2 (2003-2014). Since mid-2019, GML has
318 used a new MAGICC-3 system. This new system improved analytical techniques for CO₂, CH₄, N₂O, and
319 CO but continues to use the same GC-HePDD instruments from the older systems.

320

321 Two GC-HePDD instruments have been used for hydrogen analysis on the three flask air analysis systems
322 since 2009: H8 (MAGICC-2: 2009-2014 and MAGICC-3: August 2019-September 2020) and H11
323 (MAGICC-1: 2010-July 2019 and MAGICC-3: September 2020-present).

324 On MAGICC-1 and MAGICC-2, the H₂ instrument response was calibrated using a single tertiary
325 standard (measured before and after each sample aliquot), similar to the original 1 point calibration
326 approach used on H9.

327 Out of 17 H₂ tertiary standards used during that time, 3 were used for more than 14 months and 14
328 displayed H₂ growth over time. Figure 3 shows the calibration histories for H8 and H11 tertiary standards
329 and their start/deployment dates. For each tertiary standard, assigned mole fractions, drift coefficients, and
330 estimated uncertainties are stored in a database (SI Table 2). The uncertainty reported in SI Table 2 is
331 empirically derived and based on the standard calibration history and the standard deviation of the
332 residuals to the best fit (the assignment). The python code that calculates a secondary or tertiary standard
333 assignment uses a 0.5 ppb 1-sigma H9 reproducibility uncertainty which is added in quadrature to the
334 measurement episode standard deviation to account for longer term uncertainties not evident in the
335 standard deviation of the n-aliquots. We do not formally include an uncertainty for the secondary standard
336 assignments. The H9 reproducibility term is based on the mean of the standard deviation of residuals to
337 the fit for the calibration histories of secondary standards and target tanks over the period 2008-2022 (see
338 section 2.3.1).

339 The 17 tertiary standards used successively on the flask analysis systems between 2009 and 2019
340 introduce time dependent issues due to the variable rate of H₂ drift in aluminum tanks and the tank
341 calibration histories. Some of the tertiary standards only have pre-deployment calibration results which do
342 not assess drift during use and other standards have calibration results during their time in use but do not
343 have post deployment calibrations that may help us evaluate the drift rate for the last couple of weeks or
344 months of use (SI Table 2, notes in column “N”). Three standards exhibited an increased drift rate towards
345 the end of their life that we did not capture with their infrequent calibrations on H9. This change in drift
346 behavior was observed as increasing biases for measurements of target air tanks and daily test air flasks
347 (see section 3.1.2). We have applied offline mole fraction corrections to the flask air analysis H₂ results to

348 correct for the end of use drift increase for these three tertiary standards, and the standards' assignment
349 uncertainty is larger for these time periods (SI Table 2).

350 Since August 2019, the MAGICC-3 system operates with a GC-HePDD for H₂, new optical analyzers for
351 CO₂, CH₄ (CRDS, Picarro), CO and N₂O (QC-TILDAS, Aerodyne), and a GC-ECD for SF₆. The
352 responses of the instruments are calibrated at the same time using a single set of 11 standards spanning a
353 range of mole fractions for the six trace gases. The MAGICC-3 standards were filled at the Niwot Ridge
354 standard air preparation facility on a few different days between December 2017 and May 2018. Their H₂
355 mole fractions are regularly measured on H9 against the GML H₂ primary standards.

356 For the MAGICC-3 instrument response calibration, the eleven standards are analyzed sequentially
357 relative to an uncalibrated reference air tank (filled at Niwot Ridge). Air from each standard is injected 6
358 times alternating with the reference air. This entire sequence takes close to 17 hours. The first injection of
359 each standard is often biased low by about 2 ppb for H₂ due to timing issues at the start of each standard
360 sequence and only the remaining 5 injections are used to obtain the average normalized peak height
361 "signal" for each standard.

362 For H₂, a subset of 8 of the 11 MAGICC-3 standards are used to determine the GC-HePDD response. The
363 time-dependent H₂ value assignment for each standard was derived from 8 or 9 calibration events on H9
364 between June 2018 and December 2022 (SI Table 3, SI Figures 1 and 2). We plan on analyzing the
365 MAGICC-3 standards 2 to 3 times a year going forward. The standards' H₂ assignments will be revised as
366 needed. The three cylinders that are not used exhibit complex H₂ growth that is not well captured with
367 periodic calibration episodes and a linear or quadratic fit.

368 The time between MAGICC-3 instrument response calibration sequences was 2 weeks for the first 3
369 months of service and it has been increased to 4-5 weeks as we found the results to be quite stable. A
370 reference air cylinder will last 9 to 12 months on MAGICC-3. When the MAGICC-3 reference air
371 cylinder is changed (pressure close 250 psia), a new instrument response calibration episode is done with
372 the new reference air cylinder before flask air samples are analyzed.

373 For the asynchronous calibration to stay valid for up to 5 weeks requires the reference gas composition
374 for the six measured gases to be stable between successive calibration episodes. This has been true so far
375 except for one reference air cylinder for which a small time dependent H₂ correction was applied between
376 two instrument response calibration dates (see SI Figure 3 and more details in SI section S4).

377 **2.3 Calibration scale transfer quality assurance**

378

379 GML target air tanks are dedicated air mixtures used for measurement quality control over multiple years.
380 Most are high pressure aluminum cylinders filled at the Niwot Ridge standard preparation facility. The
381 analysis of target air helps us evaluate the robustness of the calibration scale transfer, and the consistency
382 of measurements over time and also between different analytical systems. In a perfect program, we should
383 be able to reproduce a measurement result for a target air tank every time. As noted earlier, however, the
384 reality is more complicated as H₂ tends to grow with time in aluminum cylinders. Tracking many
385 aluminum cylinders provides a diverse history of behaviors (stable, or linear vs non-linear drift), and aids
386 in the understanding of similar cylinders used for calibration.

387

388 **2.3.1 Calibration system (H9) Target air tanks**

389

390 Some GML target air cylinders are used exclusively to evaluate the stability and performance of the H9
391 measurements. Other target air cylinders are analyzed on H9 and in the flask air analysis laboratory on the
392 H8 and H11 instruments to evaluate the scale transfer.

393

394 While H₂ has been increasing in most of our target air tanks, eleven H9 target air tanks have shown either
395 stable H₂ or a linear increase less than 1 ppb/yr. Figure 4 shows the calibration histories for these tanks as
396 well as the residuals from the best fit for each tank. Table 2 has a list of these target tanks and several
397 others binned by linear drift rate. More details for target tanks are in SI Table 4. For each bin, the standard
398 deviation of the residuals (differences of the H9 calibration results minus the best fit values) is below 0.5
399 ppb. The standard deviation of the residuals for all linearly drifting target tanks binned together is 0.4 ppb.

400

401 Results for tanks with stable or very slowly drifting H₂ indicate that between 2008 and 2021, the scale
402 transfer on H9 has low uncertainty (< 1 ppb). We have eleven other target tanks for which the best fit to
403 their calibration history is a quadratic function (SI Figure 4 and SI Table 4). The standard deviation of
404 these tanks' residuals binned together is 0.7 ppb. The current set of H9 target air tank results show that
405 residuals for higher mole fraction (>650 ppb) tanks have a larger standard deviation (0.5-0.8 ppb, SI
406 Figure 4d).

407

408 Some tanks that were analyzed soon after fill and over several years show a rapid and large initial growth
409 in H₂ (in the first 0.5-2 years after fill). In this scenario, the residuals to a best linear or quadratic fit of the
410 full calibration history will be larger and will likely not capture the tank time-dependent H₂ assignment as
411 accurately. For a few of the GML standard and target air tanks, we dropped early calibration results that
412 would bias the best fit derivation and assignment during the time of use of the tank.

413

414 **2.3.2 Comparison of measurements of gas mixtures in cylinders with MPI-BGC**

415

416 Since 2016, the MPI-BGC GasLab has organized same tank air measurement (“MENI”) comparisons
417 between WMO GAW partner laboratories as part of the European ICOS (Integrated Carbon Observation
418 System) Flask and Calibration Laboratory quality control work. In this program, three 10L aluminum
419 cylinders (Luxfer UK) are filled with dry air and maintained by the MPI-BGC and sent to measurement
420 laboratories in a round robin loop. Two of the three cylinders had the same air mixture for the 2016-2021
421 period and showed small growth in their H₂ mole fractions over time. The third cylinder contains an
422 “unknown” new mixture for each round robin loop.

423

424 Between 2016 and 2021, the MENI cylinders came to GML three times and were analyzed two to four
425 times on the H9 instrument during each round robin stop. Some results were rejected due to poor
426 instrument performance or the use of an alternate calibration strategy than the one used to transfer the
427 scale. For the blind and the ambient H₂ MENI cylinders the retained NOAA H₂ results agree well with the
428 MPI_BGC measurements (< 1 ppb difference, SI Figure 5 a,b). For the low H₂ cylinder, the 2017/2018
429 NOAA measurements are biased low by about 2 ppb while the March 10, 2021 result is about 2 ppb

430 higher (SI Figure 5c). The MENI program provides a valuable on-going check for the MPI X2009 H₂
431 calibration scale transfer in GML.

432

433 2.3.3 Flask analysis systems target air tanks

434

435 Figure 5a shows the calibration histories on H9 for target air tanks used in the flask analysis laboratory
436 between 2009 and 2022. H₂ increased in all the target tanks, sometimes rapidly, requiring time dependent
437 value assignments.

438

439 Three H₂ target air tanks were in service between 2009 and 2019 and have been used to evaluate the GML
440 calibration scale transfer to the MAGICC-1 and MAGICC-2 H₂ measurements (CC1824, CB08834 and
441 CC303036). These tanks, however, exhibited rapid and large drifts and were not measured on H9 on a
442 regular basis making it more difficult to use them to evaluate potential biases on MAGICC-1 and
443 MAGICC-2 over this time period.

444

445 The target air tanks ALMX067998 and CB11143 entered into service in 2016 and 2019 respectively with
446 more frequent measurements on the calibration system to better define their time dependent value
447 assignments. A new set of six target air tanks were filled at the Niwot Ridge standard preparation facility
448 in late 2019 for the MAGICC-3 system. They have been analyzed on MAGICC-3 multiple times a year
449 but only one of them has a H₂ mole fraction that remained below 700 ppb: CB10292.

450

451 With the caveats that the non-linear drift in aluminum cylinders may not be well modeled by a simple
452 quadratic polynomial and that many of the early target tanks were under calibrated, the best polynomial fit
453 to the calibration records for all target air tanks give residuals smaller than 1.2 ppb (Figure 5b). Details for
454 the target tanks, including the best fit coefficients and the standard deviation of residuals to the fits are in
455 SI Table 5.

456

457 In Figure 6, we show the differences between the target tank analysis results on H8 and H11 and their
458 time-dependent H₂ assignments (based on the best fit to their calibration histories on H9 discussed above).
459 The differences are all within 4 ppb, however there are times when there are persistent biases between the
460 flask analysis system(s) and the calibration system. Uncertainties on the value assignment of the target air
461 tanks, the value assignments and stability of the standards used to calibrate the flask analysis systems as
462 well as the noise in the H8 and H11 measurements all contribute to the observed differences. Similar
463 offsets on both flask analysis systems (for example CC1824 prior to 2012) may point to the main
464 uncertainty contribution being from the value assignment of the target air tank. Different patterns in the
465 offsets between the two flask analysis systems (for example offsets of different signs for CC303036 and
466 CB08834 on H8 and H11 in 2011-2013) suggest the offsets are due to value assignments of the flask
467 analysis system standards. Again, this is often due to limited calibration histories not being able to fully
468 map the non-linear drift in the standards. It also indicates there are times with systematic differences
469 (mostly < 2ppb) between the MAGGIC-1/H11 and MAGICC-2/H8 measurements in the flask records.

470

471 The full transition to the new MAGICC-3 system for flask analyses in August 2019 is indicated by the
472 vertical bar in Figure 6. As discussed earlier, one improvement in this new system is that H₂
473 measurements are now calibrated using a multi-point calibration curve from a suite of standards. This

474 makes the measurement results less sensitive to drift or value assignment error in any individual standard
475 since we are fitting multiple standards. We also now appreciate the complex H₂ growth patterns that can
476 occur in aluminum cylinders so have undertaken regular calibrations to ensure drift is tracked closely.
477 These changes seem to have reduced the bias observed between the flask analysis system and the
478 calibration system, which gives confidence that future measurements will be higher quality.

479

480 To help us monitor the H₂ calibration scale propagation performance going forward, a new target air tank
481 in an Essex stainless steel cylinder, SX-1009237, was filled in late 2022 to augment the current target
482 tanks. This target air tank should be stable for H₂ and will be used for periodic comparison between
483 measurement systems. Analysis results on H9 and H11 in December 2022 are 526.75 and 527.15 ppb,
484 respectively, consistent with the residuals for other target air tanks at that time.

485

486 **3 NOAA flask air H₂ measurements**

487

488 Close to 6000 flask air samples from the NOAA Cooperative Global Air Sampling Network are analyzed
489 in GML every year. The network sites are chosen carefully to be representative of large scale air masses
490 and to be able to rely on local support for sampling and shipping logistics. The reprocessing and release
491 of the 2009-2021 H₂ global network flask air measurements on the MPI X2009 scale was made possible
492 because of continued efforts to conduct and improve the H₂ measurements, to store all the necessary data,
493 and to develop and update the tools for reliable and traceable reprocessing, comparison, and archiving.

494

495 **3.1 Data quality assurance and quality control**

496

497 In this section, we first describe the flask sample collection protocol and introduce the data quality control
498 tags used to document sample and measurement data quality issues. GML flask air H₂ measurements data
499 quality is evaluated using results from the daily analysis of test air flask pairs and from the agreement
500 between South Pole Observatory (SPO) flask pairs collected close in time. Finally, we present a
501 preliminary estimation for the uncertainty of flask air H₂ measurements over 2009-2021, that includes
502 empirical uncertainty estimates for the standards' assignments and the short-term noise of the instruments.

503

504 **3.1.1 Flask air sample collection overview and data quality tagging**

505

506 Partners in the NOAA Cooperative Global Air Sampling Network collect whole outside air samples in
507 glass flasks in pairs, upwind from any local sources of pollution, people and animals and away from
508 structures or terrain that would affect the wind flow. Two 2.5L glass flasks with two glass stopcocks with
509 Teflon o-rings are connected in series in a portable sampling unit (PSU) made of a rugged case, a battery,
510 a pump, an intake line, and a mechanism to control the pressure of the air samples. Most sampling units
511 include a dryer and are semi-automated, with the exception of those used at relatively dry high latitude
512 locations and a few other locations where a more rugged, manually operated sampling unit is required. At
513 most sites, the operator will carry the equipment outdoors to conduct the sampling. At a few sites, the
514 PSU is indoors and connected to a fixed inlet line drawing air from the outside.

515

516 Before flasks are shipped to sampling sites, the glass flasks are filled with synthetic air in the GML flask
517 logistics laboratory. During the sample collection on site, the flasks are first flushed for several minutes

518 and then filled to a pressure of 4 to 5 psi above ambient pressure in about 1 minute (See video:
519 <https://gml.noaa.gov/education/intheair.html>).

520

521 Air sample collection and/or measurement issues that are documented or detected and known to affect a
522 sample quality or an analyte measurement result are recorded with data quality control tags in our internal
523 database. For each flask air measurement, internal data quality control tags are translated into a simpler 3
524 column flag indicating if the measurement is retained or rejected for external data users. The GML flask
525 air samples and measurements can also have informational tags and comments, for example if another
526 measurement laboratory analyzed an air sample before it came to GML for analysis (see same air
527 measurement comparisons in section 3.2).

528

529 The global network flasks are filled to target pressure of 17-20 psia, but the final fill pressure can vary by
530 3-4 psi, with some of the higher altitude sites having final pressures on the lower range typically. If an air
531 sample pressure is too low for the H₂ GC instrument on the MAGICC system, the H₂ measurement result
532 is tagged as “rejected” for low sample pressure. If H₂ measurements in paired flasks have a 5 ppb or larger
533 difference, the results for the pair are tagged as rejected. If only one member of the pair had an obvious
534 issue (leak, low flask air pressure), only the H₂ measurement for that member is tagged as rejected. Some
535 issues are detected by the MAGICC performance control system and are tagged automatically. Other
536 issues are tagged manually by scientists as part of regular data quality control checks. Scientists also
537 verify the validity of the automatic tags. Members of the team routinely evaluate if follow-up actions are
538 needed to fix a sample collection or measurement issue or reduce the chance of rejecting future sample
539 results for the same issue.

540

541 Some sites can experience brief high-pollution episodes with the H₂ mole fractions in both members of a
542 pair meeting the pair agreement criteria but also being outliers, i.e. outside of the expected long-term
543 variability at the site [Novelli et al., 1999]. Gross H₂ outliers are typically “tagged” manually. A statistical
544 filter is also applied to identify outliers before each annual data release [Dlugokencky et al., 1994]. For
545 each site, a smoothing curve fit calculation determines the measurement time series mean behavior
546 broken down in a long-term trend, a seasonal cycle, and shorter-term (hours to weeks) variations
547 [Thoning et al., 1989; Tans et al., 1989a]. The code is available and a link is provided further down (see
548 Data and Code Availability section). The filter works iteratively to find and tag outlier H₂ measurements
549 when their residuals to the smooth curve fit is larger than 3 to 4 times the time series residuals’ standard
550 deviation.

551

552 **3.1.2 Test air flask analysis results**

553

554 Besides the regular analysis of target cylinders, the MAGICC flask analysis system is also tested daily
555 using flasks filled with “test air” (flasks with site code “TST”). We have four rotating high pressure
556 aluminum cylinders for test air (AL47-104, AL47-108, AL47-113, AL47-145), filled at the Niwot Ridge
557 standard preparation facility. SI Figure 6 shows their calibration histories on H₉ for different fills. H₂ is
558 not stable in the “test air” cylinders and for some tank-fills, H₂ increased rapidly and grew beyond our
559 calibration range upper limit of 700 ppb.

560

561 Every 2 to 3 weeks an even number of TST flasks (14-24) are filled from the same test air cylinder. On
562 typical analysis days, the MAGICC flask air measurement sequence will start with the analysis of air
563 from two TST flasks with the same fill date.

564

565 Global network flask air samples are analyzed at NOAA GML only during the daytime to ensure the
566 system operator is overseeing the full analysis cycle and minimizing the time a flask valve is open for the
567 analysis. This is meant to minimize the risk of losing or contaminating the air samples as many of them
568 are subsequently sent to the University of Colorado Boulder Stable Isotopes Laboratory for CO₂ and CH₄
569 isotope analyses.

570

571 Results from the TST flask pairs with the same fill date and analyzed on successive days give an
572 indication of the short-term repeatability of the measurements. Here, the deviations from the mean H₂ in
573 TST flasks with the same fill date are evaluated. For fill dates with a mean H₂ mole fraction less than 700
574 ppb, we calculate the differences between individual TST flask H₂ and the fill date mean. The standard
575 deviation of the TST flasks H₂ differences from their fill date mean is 1.39 ppb on MAGICC-2/H8
576 (N=872), 0.73 ppb on MAGICC-1/H11 (N=3583), 1.55 ppb on MAGICC-3/H8 (N=504) and 0.68 ppb on
577 MAGICC-3/H11 (N=1085), reflecting the higher measurement noise on H8.

578

579 Another diagnostic is the comparison of the TST flasks MAGICC H₂ measurement results and their test
580 air cylinders' time-dependent assignments for the dates the TST flasks were filled based on the best fit of
581 the H9 test air tank calibration results. This analysis is limited to the test air with less than 700 ppb H₂ and
582 with tank calibration results on H9 that reasonably capture the increase in H₂: AL47-108 (F), AL47-113
583 (D,E,G), AL47-145 (F,G), AL47-104 (I). In SI Figure 7 (a-c), we show the H₂ differences between the
584 TST flask results and their test air cylinder assignments. The differences reflect noise in the flask air
585 measurements and uncertainties (and potentially small biases) in the test air tank-fill assigned H₂.

586

587 Between 2010 and 2021, the three fills of test air cylinder AL47-113 are in the ambient range and have
588 the most stable H₂ mole fractions. The tank-fill assigned H₂ linear drift rate is 1 ppb/yr in fill D, null in fill
589 E and 0.4 ppb/yr in fill G. Table 3 shows the mean and standard deviation of the differences in H₂
590 between TST flasks and the assigned H₂ in a stable or slowly drifting test air tank-fill. The biases for these
591 subsets of TST air data are less than 1 ppb and the standard deviation is equal to or less than 1.5 ppb and
592 is smaller for the most recent MAGICC-3/H11 configuration, which has a smaller number of data points.

593

594 **3.1.3 South Pole Observatory: H₂ differences in flask pairs**

595

596 The South Pole Observatory (site code SPO, sampling location: 89.98°S, 24.80°W, 2810 meters above sea
597 level (masl)) gives scientists access to some of the “cleanest” air on Earth due to its remote location, and
598 thus provides an opportunity to use SPO flask data as a quality assurance tool.

599

600 Two flask pairs are typically collected weekly and close in time at the four NOAA atmospheric baseline
601 observatories using two collection methods. In method ‘S’, flasks are filled inside a building by tapping
602 the air continuously pumped for analysis on an in-situ GHG measurement system. Method ‘P’ (or ‘G’)
603 involves using a portable sampling unit with an inlet mast and pump set up outside the building, similarly
604 to other global network sites.

605

606 Staff rotation and flask shipping to and from the South Pole Observatory happen during a limited time
607 window during the Austral summer. While awaiting shipment, SPO flask air samples are stored in crates
608 in a heated storage building. Every year, one large SPO flask shipment arrives in Boulder in
609 December/January and another smaller shipment arrives in February/March. A year's worth of flasks is
610 prepared and shipped to SPO during that same time window. Despite the longer storage for SPO flasks
611 before analysis, we have not detected biases in H₂ measurements of those samples when compared with
612 other high southern latitudes times series. SPO flask air H₂ measurements show close to a 20 ppb seasonal
613 cycle and a ~15 ppb increase in the annual mean levels between 2010 and 2021 (Figure 7).

614

615 There is very little short-term variability in the surface air over Antarctica for long-lived GHGs, CO and
616 H₂. The differences in the H₂ mole fractions in SPO paired samples therefore mostly reflect the short-term
617 noise in the measurements. In SI Table 6 we report statistics for H₂ differences for the two flask sampling
618 methods and the four measurement system configurations between 2009 and 2021 with H8 and H11. As
619 observed for the TST flasks, measurements on H11 are less noisy than on H8, especially on the
620 MAGICC-3 system. The average of the absolute differences for H₂ in SPO flask paired samples is less
621 than 2 ppb ($\sigma \leq 1.3$ ppb) and methods S and P H₂ pair averages at SPO agree within 1 ppb on average (σ
622 ≤ 1.7 ppb).

623

624 **3.1.4 Flask air H₂ uncertainty estimates**

625

626 We have derived preliminary empirical uncertainty estimates for flask air H₂ measurements that fall in the
627 200-700 ppb range. For measurements on MAGICC-1 and MAGICC-2, the total uncertainty estimate
628 comes from the combination of two uncertainties added in quadrature: 1) the uncertainty on the H₂ tertiary
629 standard time-dependent assignment (SI Table 2) and 2) the instrument estimated repeatability (Table 4).
630 If an offline assignment correction is applied to take into account changes in a standard drift rate toward
631 the end of its use, the standard assignment uncertainty is increased. The H8 and H11 instrument
632 repeatability estimates are listed in Table 4. For now, we assume a 0.5 ppb uncertainty on the MAGICC-3
633 instrument response calibrated with multiple standards. On-going work will allow us to refine this last
634 uncertainty component estimate at a later date. Typical 1-sigma uncertainties for GML flask air H₂
635 measurements are 1.2 to 1.9 ppb on MAGICC-1, 1.4 to 2.8 ppb on MAGICC-2, 1.6 ppb on
636 MAGICC-3/H8 and 0.8 ppb on MAGICC-3/H11.

637 **3.2 Comparison with other GAW laboratories H₂ measurements**

638

639 A small number of laboratories operate well-calibrated long-term measurements of important atmospheric
640 trace gases. The WMO GAW coordinates regular technical and scientific discussions with experts from
641 these laboratories. Another important outcome of the WMO GAW collaborations consists of routine
642 comparisons to assess the data compatibility for measurements from different laboratories and programs
643 [Francey et al., 1999; Masarie et al., 2001; Jordan and Steinberg, 2011; Worthy et al., 2023]. The
644 WMO/GAW network compatibility goals for measurements of H₂ in well mixed background air is 2 ppb
645 (see Table 1 in [WMO/GAW, 2020]). This means that for H₂, measurement records should not have
646 persistent biases larger than 2 ppb to be used in combination with other qualifying measurements in
647 global budget, trend and large scale gradient analyses.

648

649 GML participates in several WMO GAW measurement comparison efforts. Same-flask air measurement
650 comparisons consist of one member of a NOAA flask pair collected at a site being analyzed by a partner
651 laboratory before being analyzed by GML. Co-located flask air measurement comparisons involve 2 or
652 more measurement programs having samples collected at the same location and close in time.
653 Historically, these and other “intercomparison” projects have been abbreviated ICPs, which we use in the
654 text below. Here the GML flask air H₂ measurements data compatibility is assessed with results from
655 on-going ICPs.

656

657 GML conducts same-flask air measurement comparisons at the Kennaook/Cape Grim Observatory (CGO,
658 40.68° S, 144.69° W, 164 masl) with CSIRO, Australia and at the Ochsenkopf mountain top tower (OXK,
659 50.03° N, 11.81° E, 1085 masl) with MPI-BGC, Germany. Sampling at OXK was temporarily suspended
660 between June 2019 and April 2021. The Alert/Dr Neil Trivett Observatory (ALT, 82.45° N -62.51° W,
661 190 masl) has facilitated the largest multi-laboratory flask air comparison experiment in the WMO GAW
662 program [Worthy et al., 2023]. NOAA has collocated flask air samples from ALT with CSIRO and the
663 MPI-BGC. The CSIRO and MPI-BGC H₂ measurements are also traceable to the MPI X2009 calibration
664 scale.

665

666 In Table 5, we summarize the annual mean of the differences for H₂ measurements from different
667 laboratory and flask combinations (same flask, same flask pair or collocated flasks) for CGO, OXK and
668 ALT between 2010 and 2021. All measurements included in the comparisons are retained, meaning they
669 have passed quality control checks.

670

671 Columns 2 and 3 show the annual means of the NOAA H₂ measurement differences between the ICP
672 flask and its pair mate at CGO and OXK. For CGO flask air samples collected before 2019, we find that
673 the NOAA analysis for the NOAA ICP flask first measured at CSIRO often shows higher H₂ than in the
674 non-ICP flask air sample. We suspect several of these ICP flasks had a small but detectable contamination
675 for H₂. We have applied a rejection tag to NOAA analysis results for CGO ICP flasks with an H₂ mole
676 fraction 2 ppb or more above H₂ in the non-ICP pair mate. This affected 165 ICP samples between 2009
677 and 2018 or 37% of all CGO ICP flasks collected between August 2009 and the end of 2021. For OXK,
678 the NOAA analysis result for the ICP flask first measured at MPI-BGC often shows slightly higher H₂
679 than for the non-ICP flask (Table 5, 3rd column), and the annual mean bias is less than 1 ppb for all years.

680

681 The last 4 columns in Table 5 show interlaboratory H₂ measurement comparisons for CGO, OXK and
682 ALT flask air samples. The annual mean differences are consistently less than 1.6 ppb for CGO and less
683 than 2 ppb for OXK for 9 out of 11 years (Figure 8). For collocated air samples at ALT we compare the
684 mean of flask results for each laboratory and limit the comparison for samples collected within 60
685 minutes of each other. The ALT annual mean differences vary from year to year, and are less than +/- 2
686 ppb for 8 years out of 12 for the NOAA vs CSIRO comparison and for 7 years out of 10 for the NOAA vs
687 MPI-BGC comparison. These on-going ICPs are monitored regularly to continually assess the NOAA H₂
688 data compatibility with data from GAW partners.

689

690 **4. NOAA atmospheric H₂ time series**

691 Previous measurement studies have described the H₂ global distribution for different time periods [Khalil
692 and Rasmussen, 1990; Novelli et al., 1999; Langenfelds et al., 2002; Price et al., 2007; Yver et al., 2011].
693 Some of the spatiotemporal features in the more recent NOAA H₂ measurement records are described in
694 this section.

695

696 **4.1 H₂ at the NOAA Cooperative Global Air Sampling Network Sites**

697 There are 51 sites considered active or recently terminated in the Cooperative Global Air Sampling
698 Network (see map in SI Figure 8 and site information in SI Table 7). The H₂ measurement times series for
699 these sites are shown in SI Figure 9. Note that a few sites that have been discontinued are not shown in
700 this figure. A curve fit is run for each site time series based on Thoning et al. [1989]. First the code
701 optimizes parameters for a function made of a four-term harmonic and a cubic polynomial. The resulting
702 residuals (measurements minus function) are then smoothed with a low-pass filter with a 667-day cutoff
703 and are added to the polynomial part of the function to produce the “trend curve” (shown as the dark blue
704 line in SI Figure 9). The residuals are also smoothed with a low-pass filter with a 80 day cutoff and are
705 added to the function to produce a “smooth curve” at each site.

706 The data quality control work on our long-term measurement time series includes a data selection step
707 with a statistical filter (also mentioned in section 3.1.1). Samples with H₂ beyond 3 to 4 standard
708 deviations (depending on the site) of the time series smoothed curve at a site are flagged as outliers, i.e.
709 not representative of background air conditions, and are shown as crosses in SI Figure 9.

710 The annual mean, maximum and minimum H₂ values of the smooth curve for the 51 network sites are
711 plotted in Figure 9 (in order of decreasing latitude along the x-axis) for years with retained measurements
712 up to 2021. Sampling at the TPI site, on Taiping Island, Taiwan, started in May 2019, which explains the
713 2 (full sampling year) data points for the site. Sampling at a few network sites was impacted by the
714 COVID-19 pandemic resulting in data gaps or delayed return shipping of samples. We recommend data
715 users become familiar with individual sampling site measurement records to best aggregate and interpret
716 signals.

717 The interhemispheric gradient of H₂, with higher levels in the SH, is apparent in the annual means
718 distribution across sites (Figure 9, green circles). The majority of sites in the SH (BKT to SPO on the
719 right side of Figure 9) show smaller seasonal cycle amplitudes (<23 ppb) than NH sites; however, several
720 sites have interannual variations in their H₂ seasonal cycle amplitudes (SI Figure 9). Sites with the lowest
721 H₂ seasonal minima (Figure 9, blue x symbols) likely are the most influenced by soil uptake. A few sites
722 (for ex. TAP and AMY (Republic of Korea), LLN (Taiwan), CPT (South Africa)) show higher smooth
723 curve annual maxima (Figure 9, red crosses), likely reflecting upwind local or regional emissions.

724

725 **4.2 H₂ at NOAA Baseline Atmospheric Observatories**

726

727 NOAA GML operates four staffed atmospheric baseline observatories (<https://gml.noaa.gov/obop/>). The
728 South Pole Observatory in Antarctica and the Mauna Loa (MLO, Hawaii) observatories were built in
729 connection with the 1957-1958 International Geophysical Year, a global effort bringing together 67
730 nations to study the Earth and in connection with the first launches of artificial satellites in Earth's orbit
731 by the USA and the former Soviet Union. The South Pole Observatory in Antarctica was established with
732 support from the US National Science Foundation and NOAA. The other two observatories near
733 Utqiagvik, formerly Barrow, (BRW) and Samoa (SMO) were established in 1973 and 1974 respectively.
734

735 All four NOAA atmospheric baseline observatories have an upwind clean air sector with no local sources
736 of pollution. Every week, scientists on location collect discrete air samples preferentially when the near
737 surface wind comes from the clean air sector (see earlier section 3.1.3). Figure 10 shows the reprocessed
738 H₂ time series for the Observatories between 2009 and 2021. Valid 'S' and 'P' method flask air H₂
739 measurements are retained for the South Pole Observatory only. The 'S' method flasks show
740 contaminated H₂ at Samoa and show seasonal contamination at Utqiagvik (Barrow) until August 2021
741 when sampling started at a new tower with new sampling lines. The Mauna Loa H₂ in 'S' method flasks
742 will be further evaluated and may be retained in future releases.

743 The Samoa and South Pole H₂ smooth curves show similar maximum levels between 550 and 570 ppb
744 and slightly higher minima at Samoa compared to the South Pole. The seasonal maximum occurs about 3
745 months earlier at Samoa than at the South Pole. The interannual variability is similar at both sites and is
746 dominated by 3 step increases in 2012/2013, 2016 and 2020.

747 The Mauna Loa H₂ time series shows more short-term variability than for Samoa and South Pole. The
748 seasonal cycle amplitude of the Mauna Loa H₂ smooth curve is about 40 ppb with maximum levels in
749 April-May and minimum levels in December-January. The seasonal maximum ranges from 550 to 580
750 ppb and the seasonal minimum ranges from 505 to 520 ppb. The measurements indicate that annual mean
751 H₂ levels at Mauna Loa after 2016 were higher than in previous years.

752 Of the four observatories, the Barrow H₂ time series shows the lowest levels and the strongest seasonal
753 cycle, about 60 ppb on average. The smooth curve seasonal maximum ranges from 520 to 540 ppb in
754 April-May and the seasonal minimum in September-November ranges from 450 to 490 ppb.

755 Despite having larger emissions in the NH, the H₂ interhemispheric gradient shows lower levels in the
756 extratropical NH. This is related to the larger land masses in the NH and the soil sink being the dominant
757 removal process for H₂. Warwick et al. [2022] report model-based estimates for the H₂ lifetime of 8.3
758 years for the OH sink (from the authors base model configuration) and of 2.5 years for the soil uptake
759 (average of existing literature studies). In their flux inversion, Yver et al. [2011] estimated that the NH
760 high latitudes and the tropics represent 40% and 55% of the global soil sink respectively. The soil sink
761 and OH sink in extratropical northern latitudes both peak in summertime [Price et al., 2007] leading to the
762 observed stronger H₂ minima.

763 It is important to look at data from multiple sites to study and detect interannual and potentially long-term
764 large-scale changes in atmospheric H₂ levels. In the next section, we present background air zonal mean
765 H₂ time series based on samples collected at marine boundary layer sites.

767 4.3 H₂ marine boundary layer global and zonal means

768 To extract large scale signals from the global air sampling network, we use the NOAA GML marine
769 boundary layer (MBL) zonal data product [Tans et al., 1989b; Dlugokencky et al., 1994]. Time series
770 from remote MBL sites are smoothed and interpolated to produce a latitude versus time surface of the H₂
771 mean MBL mole fraction (Figure 11). For H₂, the number of sites included in the zonal mean calculations
772 ranges from 29-42 sites until July 2017 when sampling from the Pacific Ocean shipboard (POC) was
773 stopped, after which 24-27 sites were included in the calculation (see also in Figure 9, MBL site codes
774 with an *). Because the NOAA Cooperative Global Air Sampling Network is sparse in the tropics and in
775 the SH mid latitudes, the MBL product likely does not equally detect and reflect interannual variability in
776 fluxes in these under-sampled regions, for example biomass burning emissions in Africa and South
777 America.

778 To further isolate changes in background H₂ at different latitudes, we first calculate MBL global and zonal
779 means (shown in SI Figure 10) and then derive anomalies by removing the 2010-2021 average year from
780 the global and zonal mean time series. Figure 12 shows the MBL anomaly for H₂ (black lines) and CO
781 (dashed blue lines) for the global mean and 5 zonal band means (NH and SH Polar (53-90°), NH and SH
782 Temperate (17.5-53°) and Tropics (17.5°S to 17.5°N). The NOAA GML CO measurements are for the
783 same air samples as the H₂ measurements [Pétron et al., 2023b]. Here, we derive the global and zonal
784 means for CO using the 2009-2022 MBL CO measurements and the anomalies are based on the
785 2010-2021 smooth curve zonal mean results to be consistent with the H₂ data analysis.

786 CO is emitted during incomplete combustion and is a useful marker of biomass burning emissions. CO
787 has a shorter atmospheric lifetime than H₂ which results in shorter-lived CO anomalies from pulse
788 emissions. The data reduction for the anomaly analysis is slightly different from Langenfelds et al. [2002]
789 investigation of CO₂, CH₄, H₂, and CO interannual variability in the CSIRO network 1992-1999 time
790 records. The CSIRO authors employed the same [Thoning et al., 1989] data smoothing technique as we
791 do but used the derivative of the trend curve to analyze correlations in interannual growth rate variations
792 between species. The anomaly approach chosen here allows to more closely retain the timing of abrupt
793 changes in the measurement records.

794 Over 2010-2021, background air H₂ has increased at all latitudes (Figure 12). The global mean MBL H₂
795 shows a non-uniform increase over this time with a noticeable 10 ppb step increase in 2016. The global
796 mean MBL H₂ was 20.2 ± 0.2 ppb higher in 2021 compared to 2010 (Figure 12a).

797 The meridional gradient and zonal band mean plots (Figures 11 and 12) highlight the evolution of
798 background air H₂ at different latitudes. Anomalies in the smooth curves are useful to point to time
799 periods when several successive air samples at a site show similar deviations from the average seasonal
800 cycle and multi-year trend.

801 The 2016 H₂ step increase is detected in the Tropics and SH. In the Tropics it coincides with a strong
802 positive CO anomaly that started in November 2015, reached a peak amplitude of 15 ppb mid-January
803 2016 and ended in May 2016. The 2015/2016 H₂ anomaly is first detected at Bukit Kototabang, Indonesia

804 (BKT) and later at Ascension Island (ASC), Kennaook/Cape Grim Observatory (CGO) and Crozet Island
805 (CRZ). Some BKT air samples impacted by biomass burning emissions show enhancements of 100s ppb
806 in CO and H₂ (SI Figure 11). The 2015 fire season in Indonesia was among the most intense on record as
807 shown by remote sensing products of fire counts, CO and aerosols. Field et al. [2016] found that burning
808 activities to clear peatland for farming likely contributed to larger emissions than expected from dry
809 conditions alone in 2015.

810 There is another step increase in the Polar SH zonal band in early 2020, also coinciding with a pulse
811 anomaly in CO (Figure 12f) likely related to large wildfires in Australia in late 2019-early 2020. The
812 Kennaook/Cape Grim Observatory (CGO) and Crozet Island (CRZ) smoothed curves show a large jump
813 between the late 2019 minimum and early 2020 maximum when the CGO CO measurement seasonal
814 minimum is also 10-12 ppb higher than in other years (SI Figure 11). van der Welde et al. [2021] estimate
815 that the 2019-2020 fires in Australia emitted 80% more CO₂ than “normal” Australian annual fire and
816 fossil fuel emissions combined.

817 In the NH extratropics bands, positive anomalies in H₂ in 2021 coincide with CO pulse anomalies
818 (Figures 12 b-c). For the Polar (Temperate) NH zonal band, the CO anomaly lasts from mid-July (June) to
819 December 2021 with a peak in September and an anomaly maximum amplitude of 37 ppb (19 ppb).
820 Record high emissions of CO₂ and CO from boreal forest fires in Eurasia and North America in 2021
821 have been reported by Zheng et al. [2023].

822 Previously, Simmonds et al. [2005] and Grant et al. [2010] have reported on the observed variability in
823 the Mace Head continuous H₂ measurement record and linked interannual variability in the baseline
824 annual mean H₂ to larger fire emission events. More recently, Derwent et al. [2023] shared an updated
825 analysis of the February 1994-September 2022 Mace Head in-situ H₂ measurements. The in situ record
826 shows higher monthly mean baseline H₂ levels in recent years and the authors report an increase in
827 monthly mean anomalies after December 2015 (slope of 2.4 +/- 0.5 ppb/yr). They postulate that a
828 “missing” source of increasing intensity after 2010 may be behind the observed sustained increased H₂,
829 which is markedly different from the 1998-1999 anomalies attributed to biomass burning. Derwent et al.
830 [2023] explore potential candidates for the missing sources. However, in the absence of strong and
831 quantitative direct evidence at this time, additional studies are needed to interpret the observed H₂
832 variability.

833

834 5. Conclusions

835

836 In this paper, we have described how NOAA GML has adopted the MPI X2009 H₂ calibration scale. The
837 work was confined to measurements on GC-HePDD instruments. The GML H₂ primary standards in
838 electropolished stainless steel cylinders have been calibrated once by the MPI-BGC CCL in Fall 2020.
839 We have used the CCL assignments to propagate the scale to secondary and tertiary standards. H₂
840 increases in most air standards stored in aluminum cylinders. A curve fit was applied to each standard
841 calibration history to determine a time-dependent H₂ assignment on MPI X2009. The secondary and

842 tertiary standards H₂ assignments were then used to reprocess results for NOAA flask air H₂
843 measurements on MPI X2009. The NOAA Cooperative Global Air Sampling Network flask reprocessed
844 H₂ measurements for 2009-2021 are publicly available [Pétron et al., 2023a]. For the period 2010-2021,
845 same air measurements with GAW partner laboratories have annual mean differences less than 2 ppb for
846 the Kennaook/Cape Grim Observatory comparison with CSIRO and less than 3 ppb for the Ochsenkopf
847 comparison with MPI-BGC. Over 2010-2021, background air H₂ has increased at all latitudes. However,
848 site time series and marine boundary layer H₂ zonal means show significant interannual variability. We
849 find that some of the strongest H₂ zonal mean anomalies coincide with CO anomalies and therefore were
850 likely partly driven by large biomass burning events in Indonesia (2015), Australia (2019/2020), and
851 boreal latitudes (2012 and 2021) [Field et al., 2016; Petetin et al., 2018; Zheng et al., 2023]. A full
852 analysis of the NOAA Cooperative Global Air Sampling Network H₂ measurement records is beyond the
853 scope of this paper. An early observation and global model comparison is in [Paulot et al., 2024]. The
854 NOAA H₂ dataset complements WMO GAW partner laboratories H₂ measurements and it will be
855 updated and extended routinely moving forward.

856

857 **Data and Code Availability**

858 The NOAA global network flask air H₂ and CO measurement time series are available at
859 <https://doi.org/10.15138/WP0W-EZ08>.

860

861 We kindly request that users of the NOAA H₂ dataset cite:

862 Pétron, G., Crotwell, A., Crotwell, M., Kitzis, D., Madronich, M.,
863 Mefford, T., Moglia, E., Mund, J., Neff, D., Thoning, K., & Wolter, S.
864 (2023). Atmospheric Hydrogen Dry Air Mole Fractions from the NOAA GML Carbon
865 Cycle Cooperative Global Air Sampling Network, 2009-2021 [Data set].
866 NOAA GML CCGG Division. Version: 2023-05-25, <https://doi.org/10.15138/WP0W-EZ08>

867

868 The python class used to filter and smooth time series data is available and explained at:

869 <https://gml.noaa.gov/aftp/user/thoning/ccgcrv/ccgfilt.pdf> and the method can be referenced as
870 [Thoning et al., 1989].

871

872 **Supplement**

873 The supplement for this article is available in a separate file.

874

875 **Author Contributions**

876 GP and AC designed the scale revision work. GP, AC and JM implemented the scale revision.
877 GP, AC, MC, MM, DN and JM contributed to the data quality control. GP and JP analyzed
878 network site time series. AC designed, built and oversaw the H₂ calibration scale transfer and the
879 flask air analysis system operations, working with Paul Novelli until he retired in 2017. TM and
880 AC carried out tank calibrations. BH prepared the primary standards. DK was in charge of the
881 whole air standards, reference, target and test air tanks preparation. MM and EM were
882 responsible for the flask air analysis lab operations, working with Patricia Lang until her
883 retirement in 2019. EM managed the flask logistics laboratory and flask metadata entries. DN

884 with support from SW managed the NOAA Cooperative Global Air Sampling Network. DN
885 managed sampling equipment for sites. JM manages the database and data releases. JM, KT and
886 AC developed code and user interfaces for data processing, quality control and exploration. AJ
887 calibrated the NOAA primary standards. AJ, PK and RL contributed data from their
888 measurement programs. GP prepared the manuscript with contributions from AC and AJ and
889 edits from BH, MC, RL, and JP.

890

891 **Competing Interests**

892 The authors declare that they have no conflict of interest.

893

894 **Acknowledgements**

895 We are grateful for our partners worldwide who collect and ship flask air samples to NOAA GML,
896 Boulder, CO, for analysis. We thank past and current NOAA GML and CU CIRES colleagues for their
897 contributions to the network operations, measurements, data management and data quality control. Gary
898 Morris and Kathryn McKain from GML, Simon O’Doherty and an anonymous referee provided valuable
899 comments on the manuscript.

900

901 **Financial support**

902 This work was supported in part by NOAA Cooperative Agreements NA17OAR4320101 and
903 NA22OAR4320151 and by the U.S. Department of Energy’s Office of Energy Efficiency and Renewable
904 Energy (EERE) under the Hydrogen and Fuel Cell Technologies Office (HFTO). The views expressed
905 herein do not necessarily represent the views of NOAA, the U.S. Department of Energy or the United
906 States Government.

907

908

909

910 References

911 Bertagni, M.B., Pacala, S.W., Paulot, F. et al. Risk of the hydrogen economy for atmospheric methane.

912 *Nat Commun* 13, 7706, doi: 10.1038/s41467-022-35419-7, 2022.

913 Brito J., Wurm, F., Yáñez-Serrano, A. M., de Assunção, J. V., Godoy, J. M., and Artaxo, P., Vehicular
914 Emission Ratios of VOCs in a Megacity Impacted by Extensive Ethanol Use: Results of Ambient
915 Measurements in São Paulo, Brazil, *Environmental Science & Technology*, 49 (19), 11381-11387, doi:
916 10.1021/acs.est.5b03281, 2015.

917 Ciais P., Tans, P. P., Trolier, M., et al., A Large Northern Hemisphere Terrestrial CO₂ Sink Indicated by
918 the ¹³C/¹²C Ratio of Atmospheric CO₂. *Science* 269,1098-1102, doi: 10.1126/science.269.5227.1098,
919 1995.

920 Conway, T. J., Tans, P. P., Waterman, L. S., Thoning, K. W., Kitzis, D. R., Masarie, K. A., and Zhang, N.,
921 Evidence for interannual variability of the carbon cycle from the National Oceanic and Atmospheric
922 Administration/Climate Monitoring and Diagnostics Laboratory Global Air Sampling Network, *J.*
923 *Geophys. Res.*, 99(D11), 22831–22855, doi:10.1029/94JD01951, 1994.

924 Cooper O.R., Schultz M. G., Schröder S., et al.; Multi-decadal surface ozone trends at globally distributed
925 remote locations. *Elementa: Science of the Anthropocene*; doi:10.1525/elementa.420, 2020.

926 de Kleijne, K., de Coninck H., van Zelm, R., Huijbregts M. A., and V. Hanssen S. V., The many
927 greenhouse gas footprints of green hydrogen, *Sustainable Energy Fuels*, 6, 4383-4387, doi:
928 10.1039/D2SE00444E, 2022.

929 Derwent, R. G., Simmonds, P. G., O'Doherty, S., Manning, A. J., Spain, T. G., High-frequency,
930 continuous hydrogen observations at Mace Head, Ireland from 1994 to 2022: Baselines, pollution events
931 and ‘missing’ sources, *Atmospheric Environment*, Volume 312, doi: 10.1016/j.atmosenv.2023.120029,
932 2023.

933

934 Dlugokencky, E. J., Steele, L. P., Lang, P. M., and Masarie, K. A., The growth rate and distribution of
935 atmospheric methane, *J. Geophys. Res.*, 99(D8), 17021– 17043, doi:10.1029/94JD01245, 1994.

936

937 Dlugokencky, E. J., Bruhwiler, L., White, J. W. C., et al., Observational constraints on recent increases in
938 the atmospheric CH₄ burden, *Geophys. Res. Lett.*, 36, L18803, doi:10.1029/2009GL039780, 2009.

939

940 Field, R. D., van der Werf, G. R., Fanin, T., et al., Indonesian fire activity and smoke pollution in 2015
941 show persistent nonlinear sensitivity to El Niño-induced drought. *Proceedings of the National Academy*
942 *of Sciences* 113, 33(2016), 9204–9209, doi: 10.1073/pnas.1524888113, 2016.

943

944 Francey, R. J.; Steele, L. P.; Langenfelds, R. L.; and B.C. Pak, High Precision Long-Term Monitoring of
945 Radiatively Active and Related Trace Gases at Surface Sites and from Aircraft in the Southern
946 Hemisphere Atmosphere, *Journal of Atmospheric Sciences*, pp. 279-285,
947 [https://doi.org/10.1175/1520-0469\(1999\)056%3C0279:HPLTMO%3E2.0.CO;2](https://doi.org/10.1175/1520-0469(1999)056%3C0279:HPLTMO%3E2.0.CO;2), 1999.

948

949 Francey, R. J.; Steele, L. P.; Spencer, D. A.; Langenfelds, R. L.; Law, R. M.; Krummel, P. B.; Fraser, P. J.;
950 Etheridge, D. M.; Derek, N.; Coram, S. A.; Cooper, L. N.; Allison, C. E.; Porter, L.; Baly, S. The CSIRO
951 (Australia) measurement of greenhouse gases in the global atmosphere. In: Report of the eleventh
952 WMO/IAEA Meeting of Experts on Carbon Dioxide Concentration and Related Tracer Measurement
953 Techniques; 2001; Tokyo, Japan. World Meteorological Organization; pp. 97-106.
954 <http://hdl.handle.net/102.100.100/194315>, 2003. Last accessed December 29, 2023.

955

956 Friedlingstein, P., et al., Global Carbon Budget 2022, *Earth Syst. Sci. Data*, 14, 4811–4900,
957 <https://doi.org/10.5194/essd-14-4811-2022>, 2022.

958

959 Grant, A., Witham, C. S., Simmonds, P. G., Manning, A. J., and O'Doherty, S.: A 15 year record of
960 high-frequency, in situ measurements of hydrogen at Mace Head, Ireland, *Atmos. Chem. Phys.*, 10,
961 1203–1214, doi: 10.5194/acp-10-1203-2010, 2010.

962

963 Heiskanen, J. et al., The Integrated Carbon Observation System in Europe. *Bulletin of the American*
964 *Meteorological Society* 103 (3), pp. E855 - E872, doi: 10.1175/BAMS-D-19-0364.1, 2022.

965

966 Hydrogen Council and McKinsey & Company, *Hydrogen Insights 2023*, 23pp. Accessible at:
967 <https://hydrogencouncil.com/wp-content/uploads/2023/12/Hydrogen-Insights-Dec-2023-Update.pdf>,
968 2023. Last accessed December 29, 2023.

969

970 International Energy Agency, *Global Hydrogen Review 2022*, IEA, Paris,
971 <https://www.iea.org/reports/global-hydrogen-review-2022>, License: CC BY 4.0, 284pp, 2022. Last
972 accessed December 29, 2023.

973

974 Jordan, A. and Steinberg, B.: Calibration of atmospheric hydrogen measurements, *Atmos. Meas. Tech.*, 4,
975 509–521, doi: 10.5194/amt-4-509-2011, 2011.

976

977 Khalil, M. A. K., and Rasmussen, R. A., Seasonal cycles of hydrogen and carbon monoxide in the polar
978 regions: Opposite phase relationships, *Ant. J. U. S.*, 23(5), 177-178, 1989.

979

980 Khalil, M. A. K. and Rasmussen, R. A., Global increase of atmospheric molecular hydrogen. *Nature* 347,
981 743–745, doi: 10.1038/347743a0, 1990.

982

983 Kitzis, D., *Preparation and Stability of Standard Reference Air Mixtures*, 2017.

984 <https://gml.noaa.gov/ccl/airstandard.html>. Last accessed May 17, 2023 .

985

986 Komhyr, W. D., R. H. Gammon, T. B. Harris, L. S. Waterman, T. J. Conway, W. R. Taylor, and K. W.
987 Thoning, Global atmospheric CO₂ distribution and variations from 1968–1982 NOAA/GMCC CO₂ flask
988 sample data, *J. Geophys. Res.*, 90(D3), 5567–5596, doi:10.1029/JD090iD03p05567, 1985.
989

990 Langenfelds, R. L., Francey, R. J., Pak, B. C., Steele, L. P., Lloyd, J., Trudinger, C. M., and Allison, C. E.,
991 Interannual growth rate variations of atmospheric CO₂ and its $\delta^{13}\text{C}$, H₂, CH₄, and CO between 1992 and
992 1999 linked to biomass burning, *Global Biogeochem. Cycles*, 16(3), 1048, doi:10.1029/2001GB001466,
993 2002.
994

995 Longden T., Beck, F. J., Jotzo, F., Andrews, R., Prasad, M., ‘Clean’ hydrogen? – Comparing the emissions
996 and costs of fossil fuel versus renewable electricity based hydrogen, *Applied Energy*, Volume 306, Part B,
997 118145, ISSN 0306-2619, doi: 10.1016/j.apenergy.2021.118145, 2022.
998

999 Masarie, K. A., Langenfelds, R. L., Allison, C.E., et al., NOAA/CSIRO Flask Air Intercomparison
1000 Experiment: A strategy for directly assessing consistency among atmospheric measurements made by
1001 independent laboratories, *J. Geophys. Res.*, 106(D17), 20445–20464, doi:10.1029/2000JD000023, 2001.
1002

1003 Montzka, S.A., Dutton, G.S., Yu, P. et al. An unexpected and persistent increase in global emissions of
1004 ozone-depleting CFC-11. *Nature* 557, 413–417, doi: 10.1038/s41586-018-0106-2, 2018.
1005

1006 Novelli, P. C., Elkins, J.W., Steele, L. P., The Development and Evaluation of a Gravimetric Reference
1007 Scale For Measurements of Atmospheric Carbon Monoxide, *J. Geophys. Res.*, 96, 13,109-13,121, doi:
1008 10.1029/91JD01108, 1991.
1009

1010 Novelli, P. C., Steele, L. P., and Tans, P. P., Mixing ratios of carbon monoxide in the troposphere, *J.*
1011 *Geophys. Res.*, 97, 20,731-20,750, doi:10.1029/92JD02010, 1992.
1012

1013 Novelli, P. C., Lang, P. M., Masarie, K. A., Hurst, D. F., Myers, R., and W., E. J.: Molecular hydrogen in
1014 the troposphere: Global distribution and budget, *J. Geophys. Res.*, 104, 30427–30444, doi:
1015 10.1029/1999JD900788, 1999.
1016

1017 Novelli, P. C., Crotwell, A. M., and Hall, B. D., Application of Gas Chromatography with a Pulsed
1018 Discharged Helium Ionization Detector for Measurements of Molecular Hydrogen, *Env. Sci. Technol.*
1019 (43), 2431-2436, doi: 10.1021/es803180g, 2009.
1020

1021 Ocko, I. B. and Hamburg, S. P.: Climate consequences of hydrogen emissions, *Atmos. Chem. Phys.*, 22,
1022 9349–9368, doi: 10.5194/acp-22-9349-2022, 2022.
1023

1024 Oltmans S. J. and Levy, H. II, Surface ozone measurements from a global network,
1025 *Atmospheric Environment*, Volume 28, Issue 1, Pages 9-24, ISSN 1352-2310, doi:
1026 10.1016/1352-2310(94)90019-1, 1994.
1027

1028 Paulot, F., Pétron, G., Crotwell, A. M., and Bertagni, M. B.: Reanalysis of NOAA H₂ observations:
1029 implications for the H₂ budget, *Atmos. Chem. Phys.*, 24, 4217–4229, doi: 10.5194/acp-24-4217-2024,
1030 2024.
1031

1032 Petetin, H., Sauvage, B., Parrington, M., Clark, H., Fontaine, A., Athier, G., Blot, R., Boulanger, D.,
1033 Cousin, J.-M., Nédélec, P., and Thouret, V.: The role of biomass burning as derived from the
1034 tropospheric CO vertical profiles measured by IAGOS aircraft in 2002–2017, *Atmos. Chem. Phys.*,
1035 18, 17277–17306, doi: 10.5194/acp-18-17277-2018, 2018.
1036

1037 Pétron, G., et al., Hydrocarbon emissions characterization in the Colorado Front Range: A pilot
1038 study, *J. Geophys. Res.*, 117, D04304, doi:10.1029/2011JD016360, 2012.
1039

1040 Pétron, G., Crotwell, A., Crotwell, M., Kitzis, D., Madronich, M., Mefford, T., Moglia, E., Mund, J., Neff,
1041 D., Thoning, K., & Wolter, S., Atmospheric Hydrogen Dry Air Mole Fractions from the NOAA GML
1042 Carbon Cycle Cooperative Global Air Sampling Network, 2009–2021 [Data set]. NOAA GML CCGG
1043 Division. Version: 2023-05-25, doi: 10.15138/WP0W-EZ08, 2023a.
1044

1045 Pétron G., A.M. Crotwell, M.J. Crotwell, E. Dlugokencky, M. Madronich, E. Moglia, D. Neff, K.
1046 Thoning, S. Wolter, J.W. Mund, Atmospheric Carbon Monoxide Dry Air Mole Fractions from the
1047 NOAA GML Carbon Cycle Cooperative Global Air Sampling Network, 1988–2022, Version:
1048 2023-08-28, doi: 10.15138/33bv-s284, 2023b.
1049

1050 Price, H., Jaegle, L., Rice, A., Quay, P., Novelli, P. C., and Gammon, R.: Global budget of molecular
1051 hydrogen and its deuterium content: Constraints from ground station, cruise, and aircraft observations, *J.*
1052 *Geophys. Res.*, 112, D22108, doi:10.1029/2006JD008152, 2007.
1053

1054 Propper, R., Wong, P., Bui, S., Austin, J., Vance, W., Alvarado, Á., Croes, B., and Luo, D., Ambient and
1055 Emission Trends of Toxic Air Contaminants in California, *Environmental Science & Technology*, 49 (19),
1056 11329–11339, doi: 10.1021/acs.est.5b02766, 2015.
1057

1058 Schultz, M.G., Akimoto, H., Bottenheim, J., et al., The Global Atmosphere Watch reactive gases
1059 measurement network. *Elementa: Science of the Anthropocene*, 3, doi:
1060 10.12952/journal.elementa.000067, 2015.
1061

1062 Simmonds, P. G., Derwent, R. G., O’Doherty, S., Ryall, D. B., Steele, L. P., Langenfelds, R. L., Salameh,
1063 P., Wang, H. J., Dimmer, C. H., and Hudson, L. E.: Continuous high-frequency observations of hydrogen
1064 at the Mace Head baseline atmospheric monitoring station over the 1994–1998 period, *J. Geophys. Res.*,
1065 105, 12105–12121, doi: 10.1029/2000JD900007, 2000.
1066

1067 Simmonds, P. G., A.J. Manning, R.G. Derwent, P. Ciais, M. Ramonet, V. Kazan, D. Ryall,
1068 A burning question. Can recent growth rate anomalies in the greenhouse gases be attributed to large-scale
1069 biomass burning events?, *Atmospheric Environment*, Volume 39, Issue 14, Pages 2513–2517, doi:
1070 10.1016/j.atmosenv.2005.02.018, 2005.
1071

1072 Simpson, I.J., M.P.S. Andersen, S. Meinardi, L. Bruhwiler, N.J. Blake, et al., Long-term decline of global
1073 atmospheric ethane concentrations and implications for methane. *Nature*, 488(7412):490–494, doi:
1074 10.1038/nature11342, 2012.

1075

1076 Steele, L.P., Fraser, P.J., Rasmussen, R.A. et al. The global distribution of methane in the troposphere. *J*
1077 *Atmos Chem* 5, 125–171, doi: 10.1007/BF00048857, 1987.

1078

1079 Storm, I., Karstens, U., D'Onofrio, C., Vermeulen, A., and Peters, W.: A view of the European carbon flux
1080 landscape through the lens of the ICOS atmospheric observation network, *Atmos. Chem. Phys.*, 23,
1081 4993–5008, doi: 10.5194/acp-23-4993-2023, 2023.

1082 Tans, P.P., Thoning, K.W., Elliot, W.P., and Conway, T.J., *Background atmospheric CO₂ patterns from*
1083 *weekly flask samples at Barrow, Alaska: Optimal signal recovery and error estimates*, NOAA Tech.
1084 Memo. (ERL-ARL-173). Environ. Res. Lab., Boulder, Colo., 131 pp. 1989a.

1085 Tans, P.P., T.J. Conway, and T. Nakazawa, Latitudinal distribution of the sources and sinks of atmospheric
1086 carbon dioxide derived from surface observations and an atmospheric transport model, *J. Geophys. Res.*,
1087 94, 5151-5172, doi: 10.1029/JD094iD04p05151, 1989b.

1088 Thompson A. M., J. C. Witte, S. J. Oltmans, F. J. Schmidlin, SHADOZ - A tropical
1089 ozonesonde-radiosonde network for the atmospheric community. *Bulletin of the American Meteorological*
1090 *Society*, Vol. 85, No. 10, pp. 1549-1564, <http://www.jstor.org/stable/26221206>, 2004.

1091 Thoning, K.W., P.P. Tans, and W.D. Komhyr, Atmospheric carbon dioxide at Mauna Loa Observatory 2.
1092 Analysis of the NOAA GMCC data, 1974-1985, *J. Geophys. Res.*, 94, 8549-8565, doi:
1093 10.1029/JD094iD06p08549, 1989.

1094 Tørseth, K., Aas, W., Breivik, K., Fjæraa, A. M., Fiebig, M., Hjellbrekke, A. G., Lund Myhre, C.,
1095 Solberg, S., and Yttri, K. E.: Introduction to the European Monitoring and Evaluation Programme
1096 (EMEP) and observed atmospheric composition change during 1972–2009, *Atmos. Chem. Phys.*, 12,
1097 5447–5481, doi: 10.5194/acp-12-5447-2012, 2012.

1098 van der Velde, I.R., van der Werf, G.R., Houweling, S. *et al.* Vast CO₂ release from Australian fires in
1099 2019–2020 constrained by satellite. *Nature* 597, 366–369, doi: 10.1038/s41586-021-03712-y, 2021.

1100 von Schneidmesser E., Monks, P.S., Plass-Duelmer C., Global comparison of VOC and CO observations
1101 in urban areas, *Atmospheric Environment*, Volume 44, Issue 39, Pages 5053-5064, ISSN 1352-2310, doi:
1102 10.1016/j.atmosenv.2010.09.010, 2010.

1103 Yver, C. E., Pison, I. C., Fortems-Cheiney, A., A new estimation of the recent tropospheric molecular
1104 hydrogen budget using atmospheric observations and variational inversion, *Atmos. Chem. Phys.*, 11,
1105 3375–3392, doi: 10.5194/acp-11-3375-2011, 2011.

1106 Warwick, N., Griffiths, P., Keeble, J., Archibald A., Pyle, J., and Shine, K.: Atmospheric implications of
1107 increased Hydrogen use, UK government's Department of Business, Energy and Industrial Strategy
1108 (BEIS) report, 2022. Accessible at:

1109 <https://assets.publishing.service.gov.uk/media/624eca7fe90e0729f4400b99/atmospheric-implications-of-i>
1110 ncreased-hydrogen-use.pdf, Last accessed: October 18, 2023.

1111

1112 Warwick, N. J., Archibald, A. T., Griffiths, P. T., Keeble, J., O'Connor, F. M., Pyle, J. A., and Shine, K. P.:
1113 Atmospheric composition and climate impacts of a future hydrogen economy, *Atmos. Chem. Phys.*, 23,
1114 13451–13467, <https://doi.org/10.5194/acp-23-13451-2023>, 2023.

1115 World Meteorological Organization, Global Atmospheric Watch, 20th WMO/IAEA Meeting on Carbon
1116 Dioxide, Other Greenhouse Gases and Related Measurement Techniques (GGMT-2019), report 255,
1117 2020. Accessible at:

1118 <https://library.wmo.int/records/item/57135-20th-wmo-iaea-meeting-on-carbon-dioxide-other-greenhouse->
1119 [gases-and-related-measurement-techniques-ggmt-2019](https://library.wmo.int/records/item/57135-20th-wmo-iaea-meeting-on-carbon-dioxide-other-greenhouse-). Last accessed: December 4, 2023.

1120 World Meteorological Organization, Greenhouse Gas Bulletin (18): The State of Greenhouse Gases in the
1121 Atmosphere Based on Global Observations through 2021. 10p., 2022. Accessible at:

1122 <https://library.wmo.int/idurl/4/58743>. Last accessed: January 2, 2024.

1123 Worthy, D. E. J., Rauh, M. K., Huang, L., et al., Results of a Long-Term International Comparison of
1124 Greenhouse Gas and Isotope Measurements at the Global Atmosphere Watch (GAW) Observatory in
1125 Alert, Nunavut, Canada, *Atmos. Meas. Tech.*, 16, 5909–5935, doi: 10.5194/amt-16-5909-2023, 2023.

1126 Yap, J., and McLellan B. A., Historical Analysis of Hydrogen Economy Research, Development, and
1127 Expectations, 1972 to 2020, *Environments*, 10, 11, doi: 10.3390/environments10010011, 2023.

1128 Zheng, B., Ciais, P., Chevallier, F., et al., Record-high CO₂ emissions from boreal fires in 2021. *Science*,
1129 379, 912-917, doi: 10.1126/science.ade0805, 2023.

1130

1131 **Tables**

1132

1133 Table 1. NOAA GML H₂ primary standards (prepared gravimetrically) and their WMO/MPI X2009

1134 assignments (dated 2022-02-28). All H₂ dry air mole fractions and their uncertainties are in ppb.

Serial Number	Fill code	Fill Date	CCL value	CCL uncertainty
SX-3558	A	2008-10-17	248.4	0.1
SX-0614470	A	2019-04-15	352.8	0.1
SX-3543	B	2008-11-03	425.4	0.2
SX-3540	B	2007-08-07	488	0.2
SX-0614471	A	2019-04-19	496.5	0.3
SX-3523	C	2007-07-24	527	0.2
SX-3554	A	2007-08-02	601.2	0.2
SX-0614472	A	2019-04-19	701.9	0.2

1135

1136

1137

1138

1139 Table 2: H9 Target air tanks with zero or linear growth in H₂

Linear Drift Rate (ppb/yr)	Target Tank IDs	Standard deviation of residuals to best fits (ppb)
0	CA05278, CA06194, CA08247, CC121971, CC311842 ND16439, ND33960	0.46
0-1	ALM-065166, CA05300, CC71607, CC73110	0.42
2-5	CA04551, CA07328, CB10910	0.32
5-10	CC71579	0.36
> 20	CA08145	0.48

1140

1141

1142

1143 Table 3. Summary statistics for H₂ differences between test air tank-fill assignment (based on H9
 1144 calibration history) and associated TST flask measurements on MAGICC systems

System / Instrument	Test air tank id and fill	Differences mean (ppb)	Differences standard deviation (ppb)	Number of samples
MAGICC-2 / H8	AL47-113 D, E	-0.3	1.3	528
MAGICC-1 / H11	AL47-113 D, E, G	+0.3	1.1	1231
MAGICC-3 / H8	AL47-145 G	-0.9	1.5	388
MAGICC-3 / H11	AL47-113 G	+0.4	0.6	144

1145

1146

1147

1148 Table 4: Flask air H₂ measurement uncertainty components

Uncertainty components	1 sigma uncertainty estimate (ppb)	Source
Tertiary standard time-dependent assignment uncertainty (1 point calibration)	0.5-2.5 Tank specific (see SI Table 2)	Calibration histories, residuals to best fit, TST flasks
MAGICC-3 response curve uncertainty	0.5	Preliminary estimate, will be reassessed.
Measurement repeatability on H8	1.3 (MAGICC-2) 1.5 (MAGICC-3)	TST and SPO flask pair differences (Table 3 and SI Table 6)
Measurement repeatability on H11	1.1 (MAGICC-1) 0.6 (MAGICC-3)	

1149

1150 Table 5: Annual mean of H₂ measurement differences (in ppb) for air samples from the Kennaook/Cape
 1151 Grim Observatory (CGO), Ochsenkopf (OXK) and Alert (ALT). Non background air sample
 1152 measurement results are included. Colocated (not same air) samples at ALT are matched within a +/- 60
 1153 minutes window.

1154

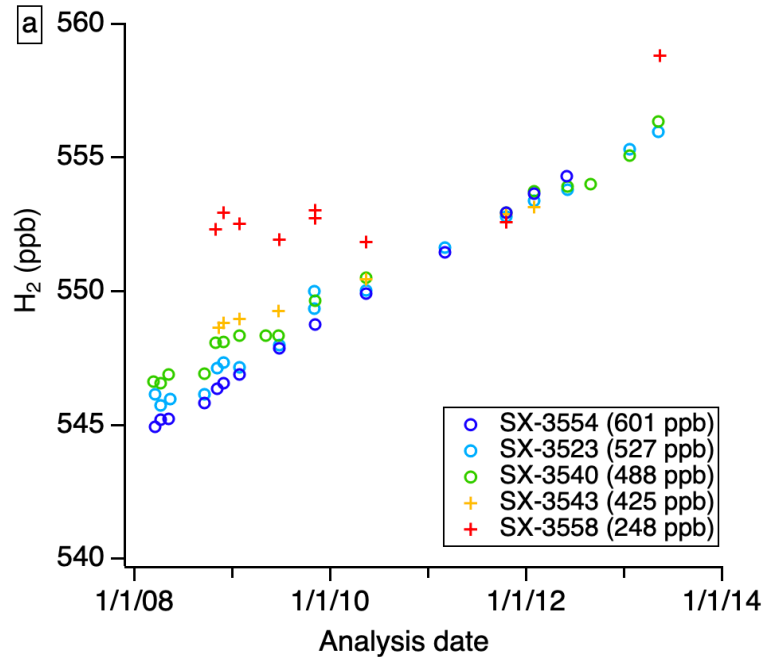
Year	NOAA ICP-NOAA nonICP		CGO NOAA non ICP minus CSIRO ICP	OXK NOAA ICP minus MPI ICP	ALT NOAA minus CSIRO (not same air)	ALT NOAA minus MPI (not same air)
	CGO*	OXK				
2010	-	-0.05	0.72	-0.17	-3.4	-3.5
2011	-	0.15	0.50	-0.02	2.2	-3.9
2012	0.58	0.13	0.40	-0.29	0.66	-2.3
2013	-	0.01	0.23	0.80	1.30	-1.4
2014	-	0.19	1.37	1.61	0.63	-1.1
2015	-	0.85	0.02	0.53	0.52	-1.4
2016	1.32	0.20	1.54	2.91	-0.32	-1.4
2017	1.19	0.56	1.38	2.49	3.2	-
2018	0.91	0.53	1.31	1.69	1.2	-1.3
2019	0.73	-0.07	0.30	1.25	1.0	-0.81
2020	0.18	na	0.19	-	0.01	-0.22
2021	0.33	0.33	0.86	1.71	3.4	-

1155 *Most NOAA ICP flasks from CGO had a small contamination for CO and H₂ prior to 2019. If the
 1156 NOAA ICP flask H₂ results are > 2ppb larger than the NOAA non-ICP flask H₂ in the pair, the ICP flask
 1157 H₂ has been rejected. Only years with at least 10 valid H₂ pairs are included.

1158 **Figures**

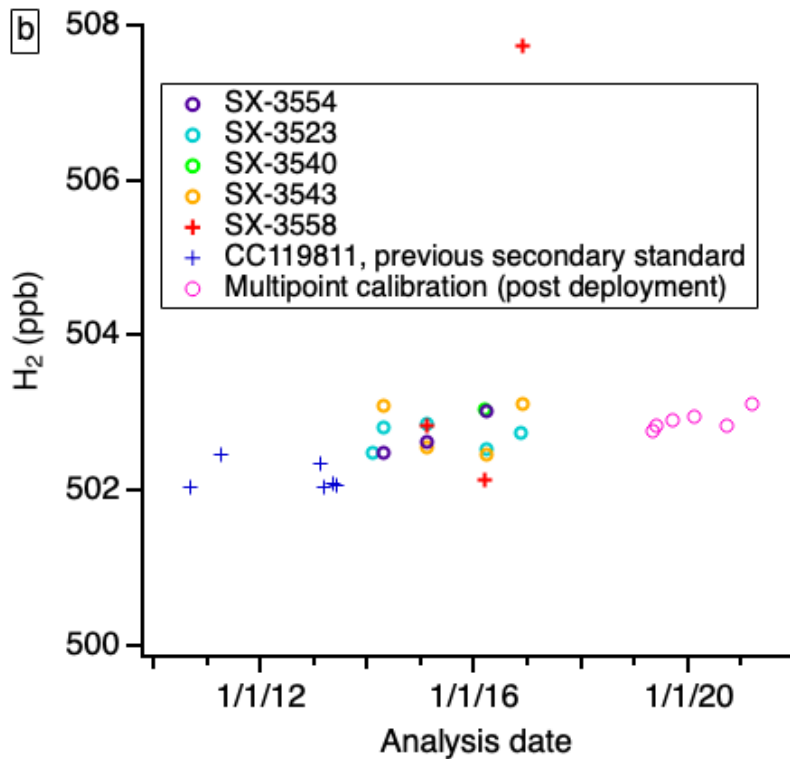
1159

1160 Figure 1. Calibration results for GML two H₂ secondary standards (a) CC119811 and b) CA03233 on H9
1161 against one of the primary standards. 2019-2020 multipoint calibration results on H9 are also shown for
1162 CA03233 (pink circles). Only results shown with open circles are used for the assignments.



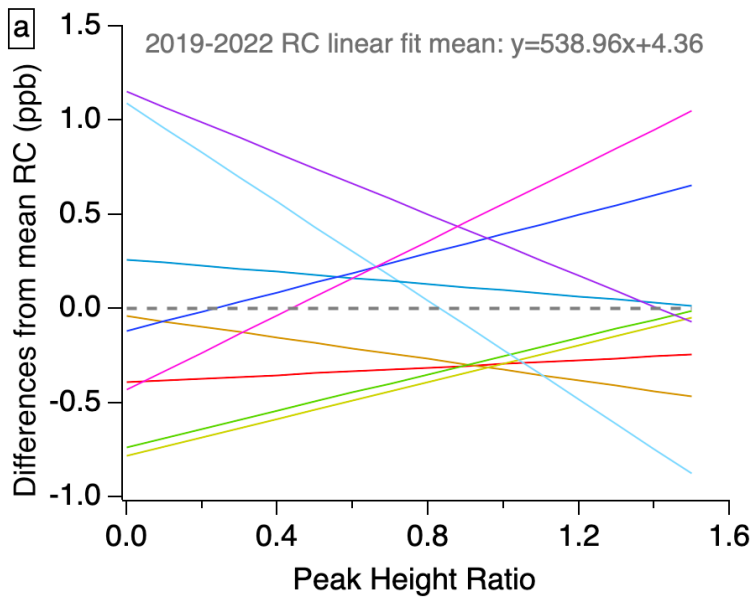
1163

1164

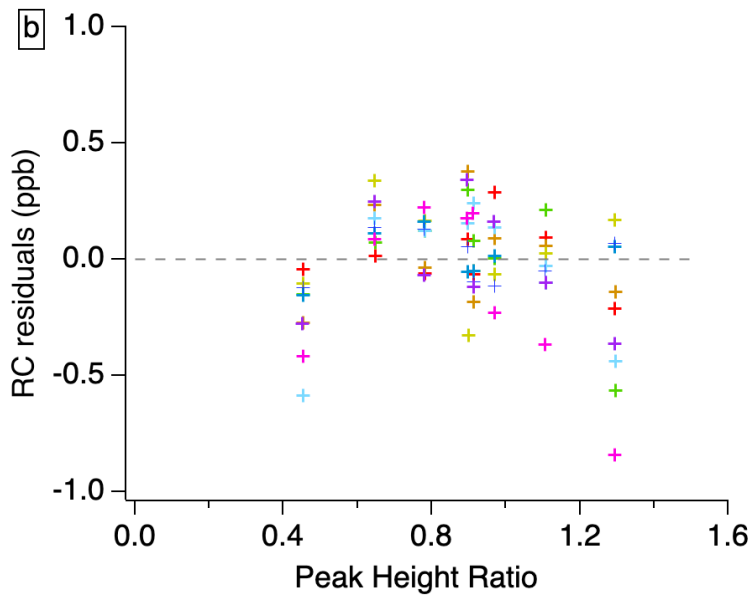


1165

1166 Figure 2: 2019-2022 H9 standard calibration response curve (RC) results: a) differences from the mean
1167 RC linear fit and b) residuals of the response curve fits. Different colors are for different calibration
1168 episodes.
1169

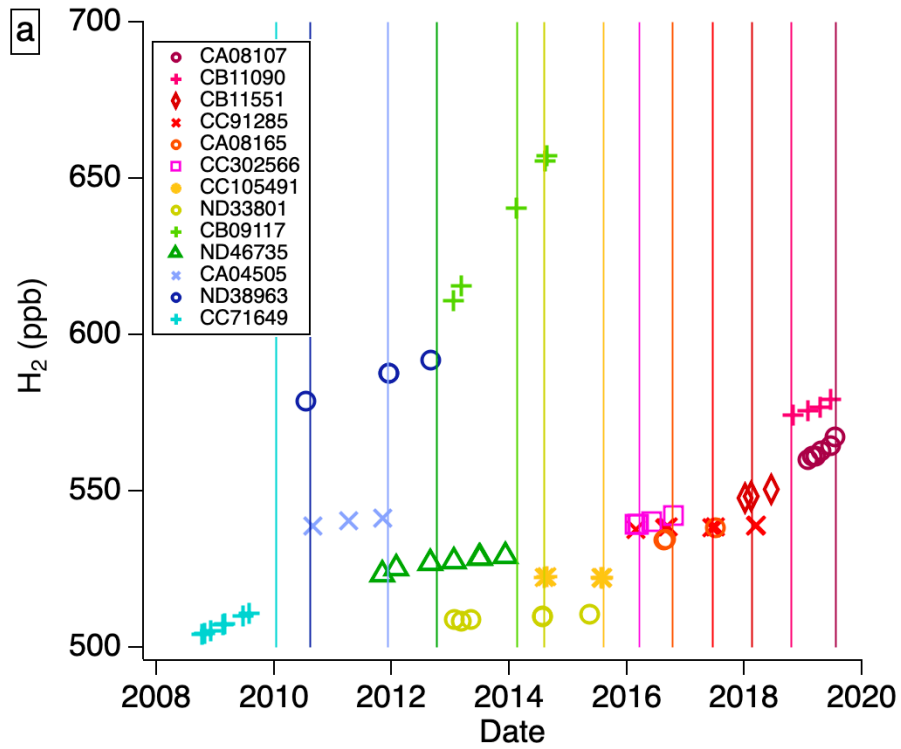


1170
1171

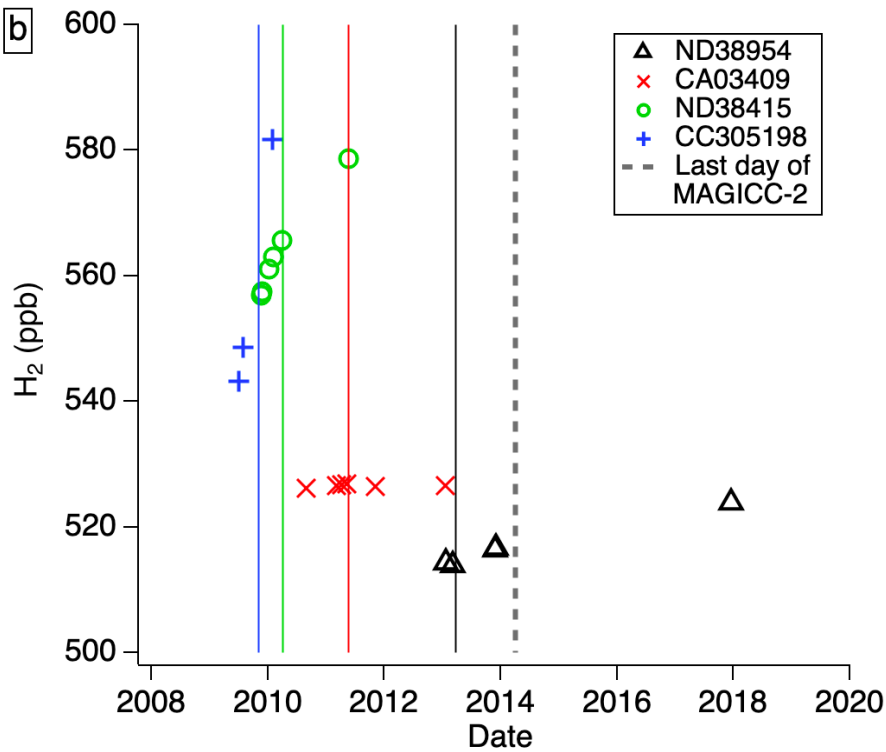


1172
1173
1174
1175
1176

1177 Figure 3. Calibration histories of a) MAGICC-1 / H11 and b) MAGICC-2 / H8 tertiary standards. The
 1178 colored vertical line indicates when a standard started to be used.
 1179



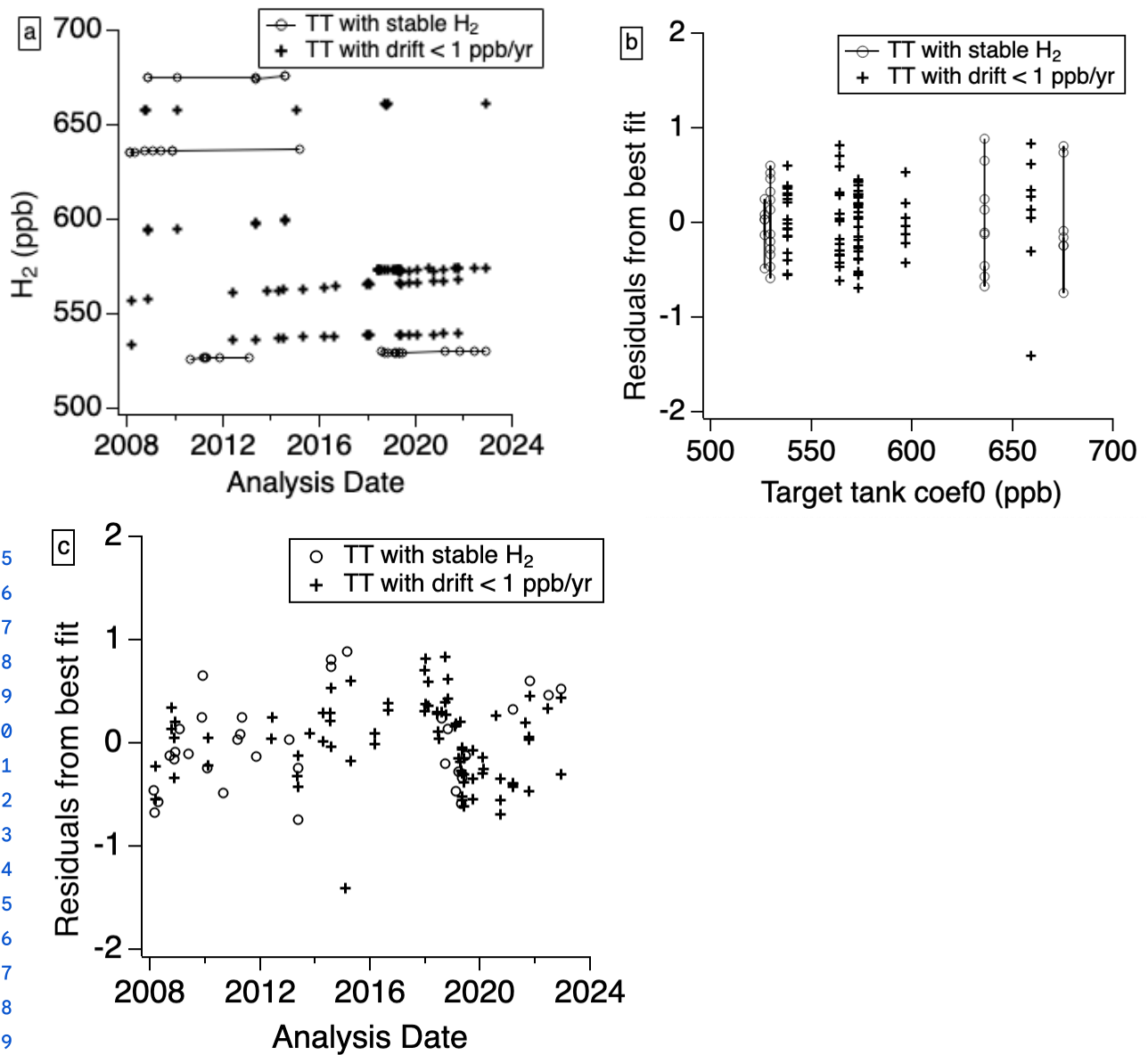
1180



1181

1182

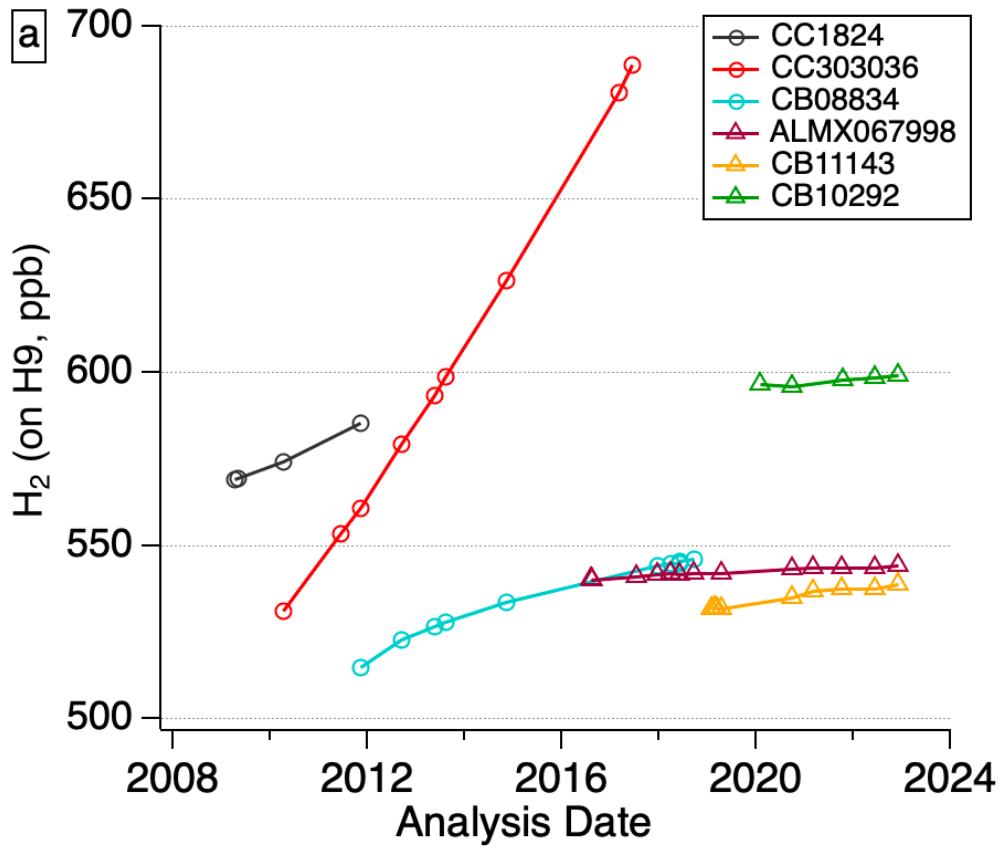
1183 Figure 4: Calibration histories and residuals to best fit for H9 target tanks with a stable H₂ mole fraction
1184 or a linear drift less than 1 ppb/yr. Residuals are in ppb.



1185
1186
1187
1188
1189
1190
1191
1192
1193
1194
1195
1196
1197
1198
1199
1200
1201
1202
1203

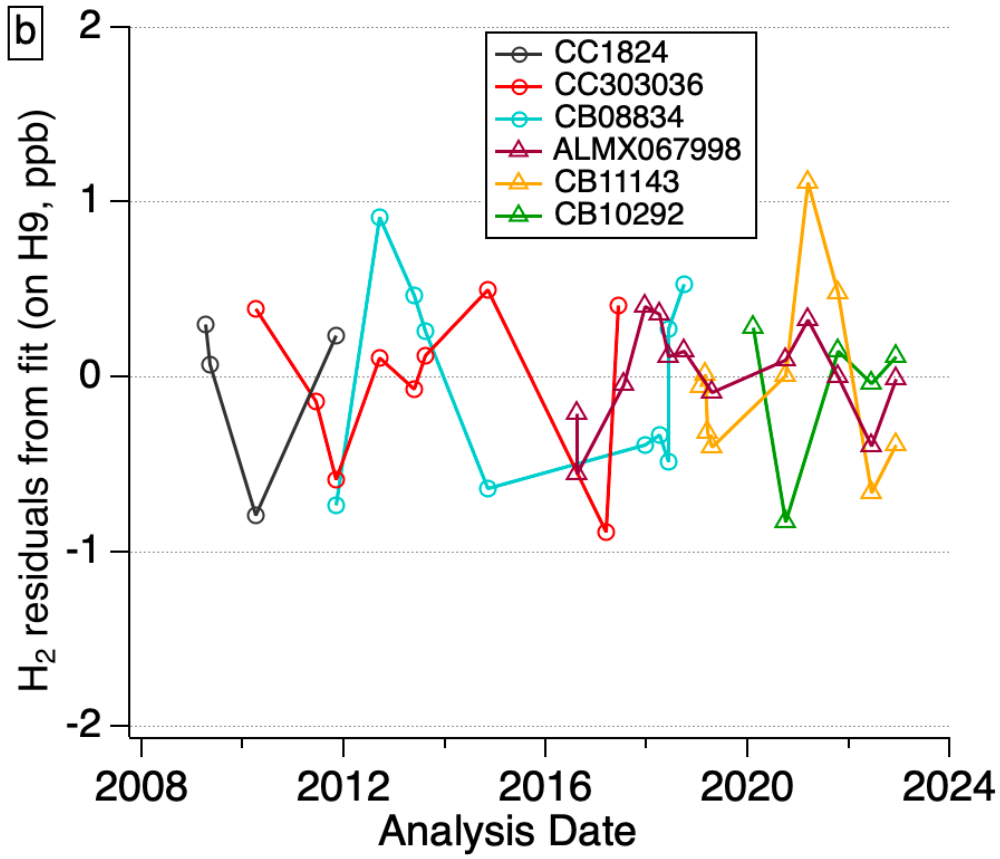
1204 Figure 5. Flask air analysis systems target air tanks H9 a) calibration histories and b) residuals to best
1205 linear or quadratic fit.

1206



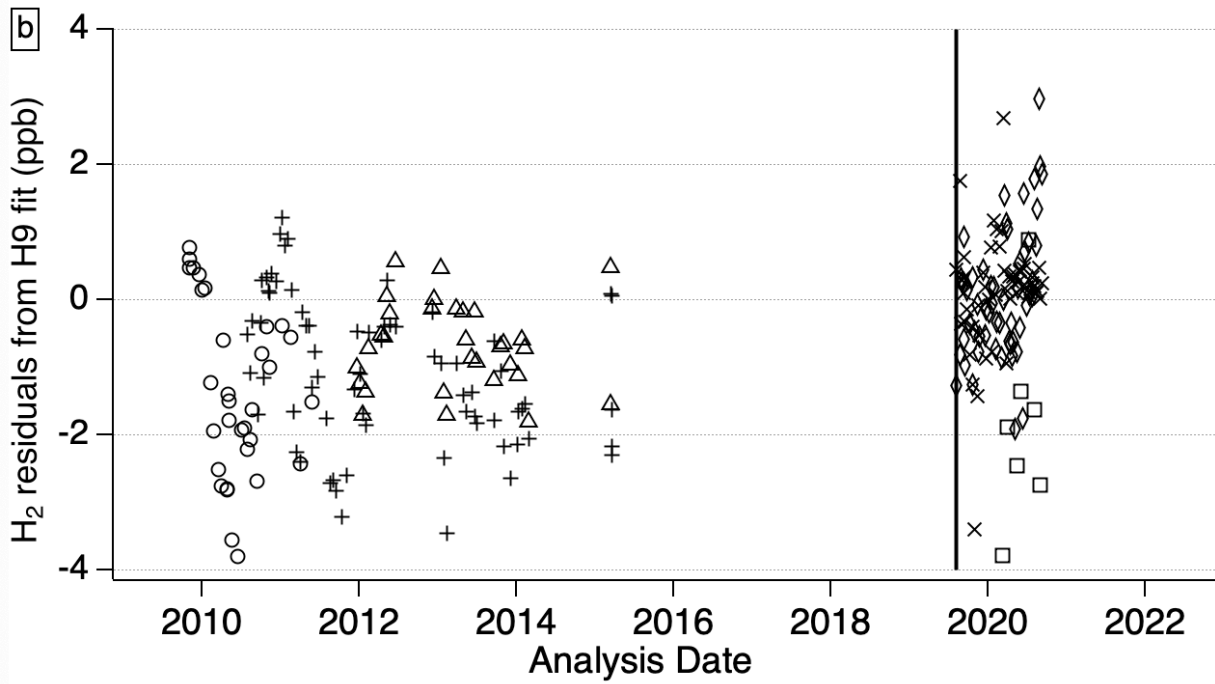
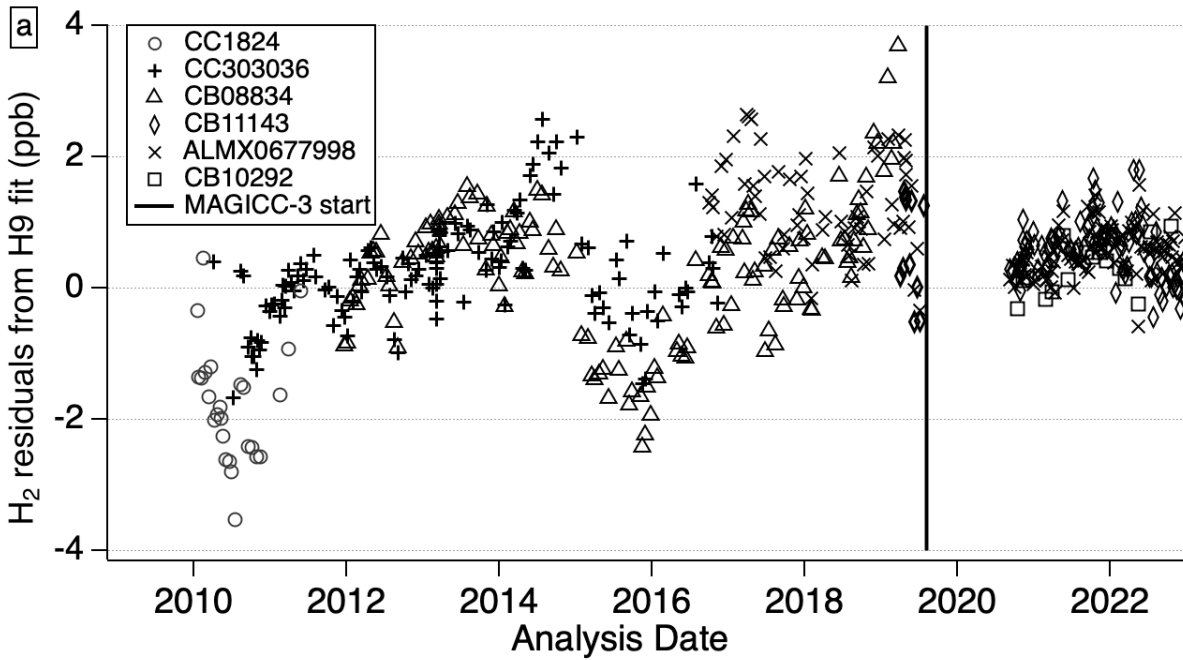
1207

1208



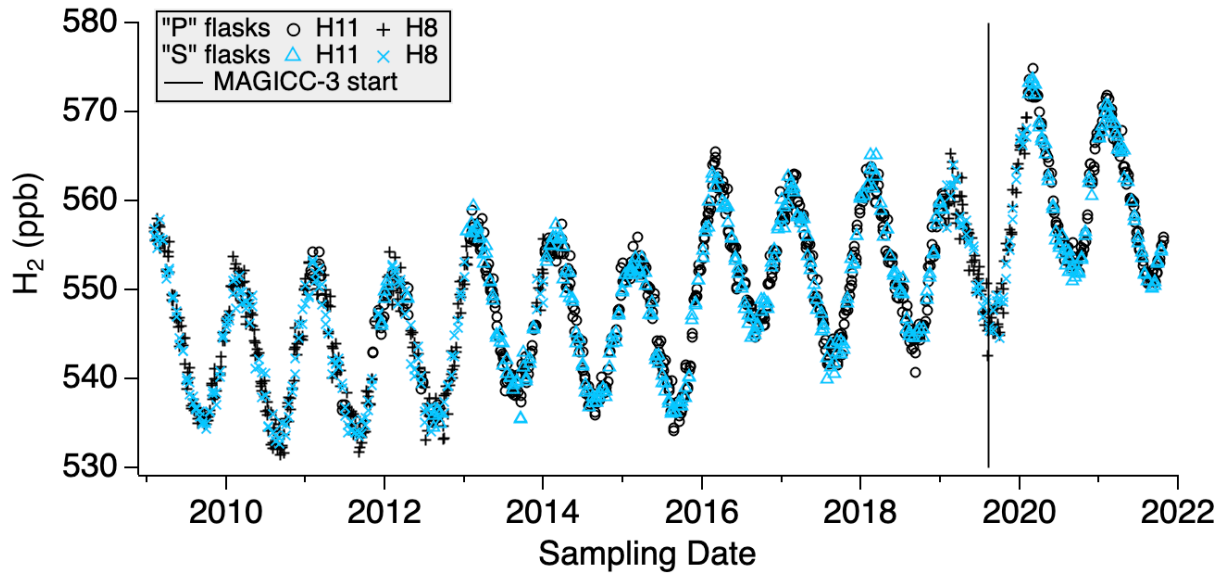
1209
 1210
 1211
 1212
 1213
 1214
 1215
 1216
 1217
 1218
 1219
 1220
 1221
 1222
 1223
 1224
 1225
 1226
 1227
 1228
 1229

1230 Figure 6. Differences of target air tank H₂ analysis results on a) H11 and b) H8 and the time-dependent
1231 assignment based on calibration history on H9.



1233
1234
1235

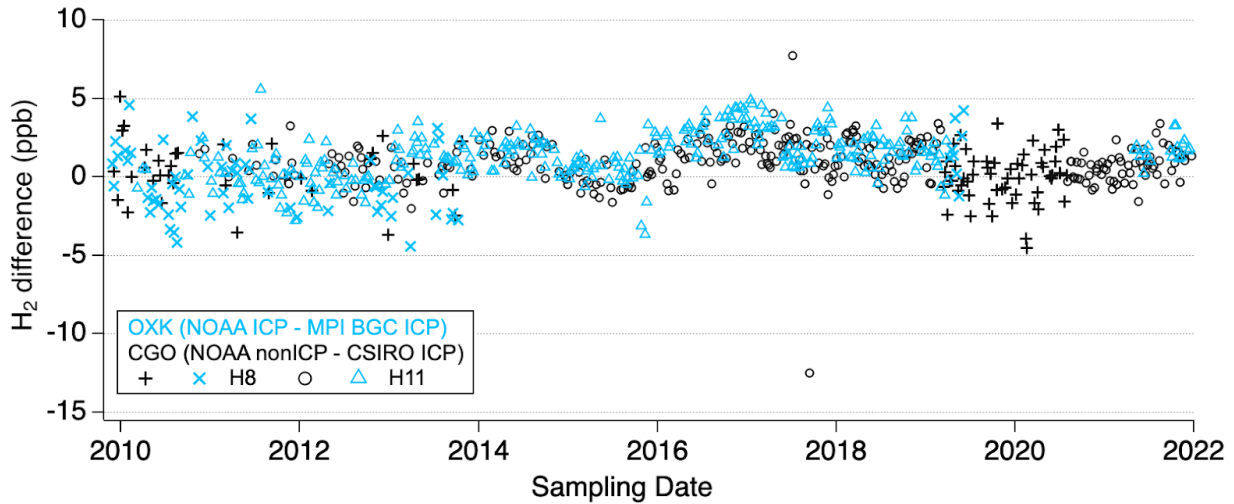
1236 Figure 7. South Pole Observatory flask air H₂ measurements on H11 and H8. Black symbols are used for
 1237 measurements of P flasks and blue symbols are used for measurements of S flasks.



1238

1239 Figure 8. Interlaboratory same air H₂ measurement difference for OXK ICP (NOAA - MPI-BGC) and
 1240 CGO (NOAA non ICP - CSIRO ICP).

1241



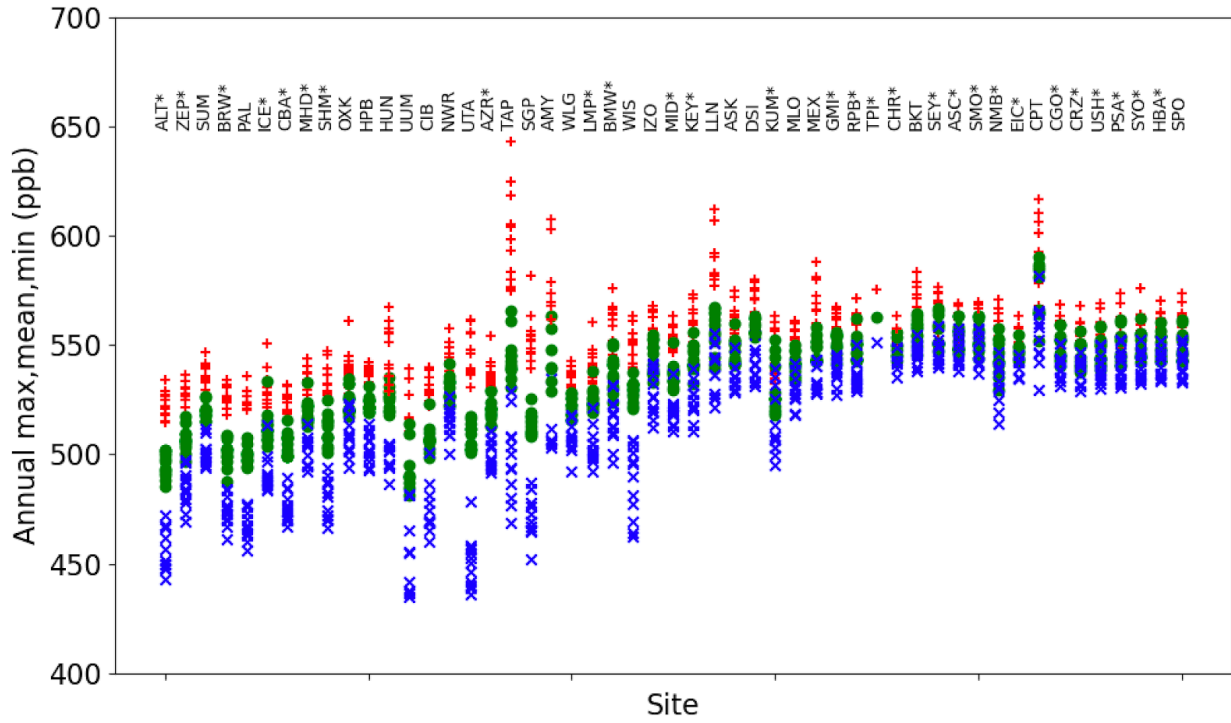
1242

1243

1244

1245 Figure 9: Annual maximum (red), mean (green) and minimum (blue) H₂ from the smooth curve fit of the
 1246 2010-2021 measurement time series for each surface site in the global sampling network. Each site is
 1247 referred to with a three letter code (see details in SI Table 7). The sampling sites are shown along the
 1248 x-axis with decreasing latitudes. An asterisk near the site code indicates if the site data are used for the
 1249 marine boundary layer air zonal and global means H₂ data reduction.

1250

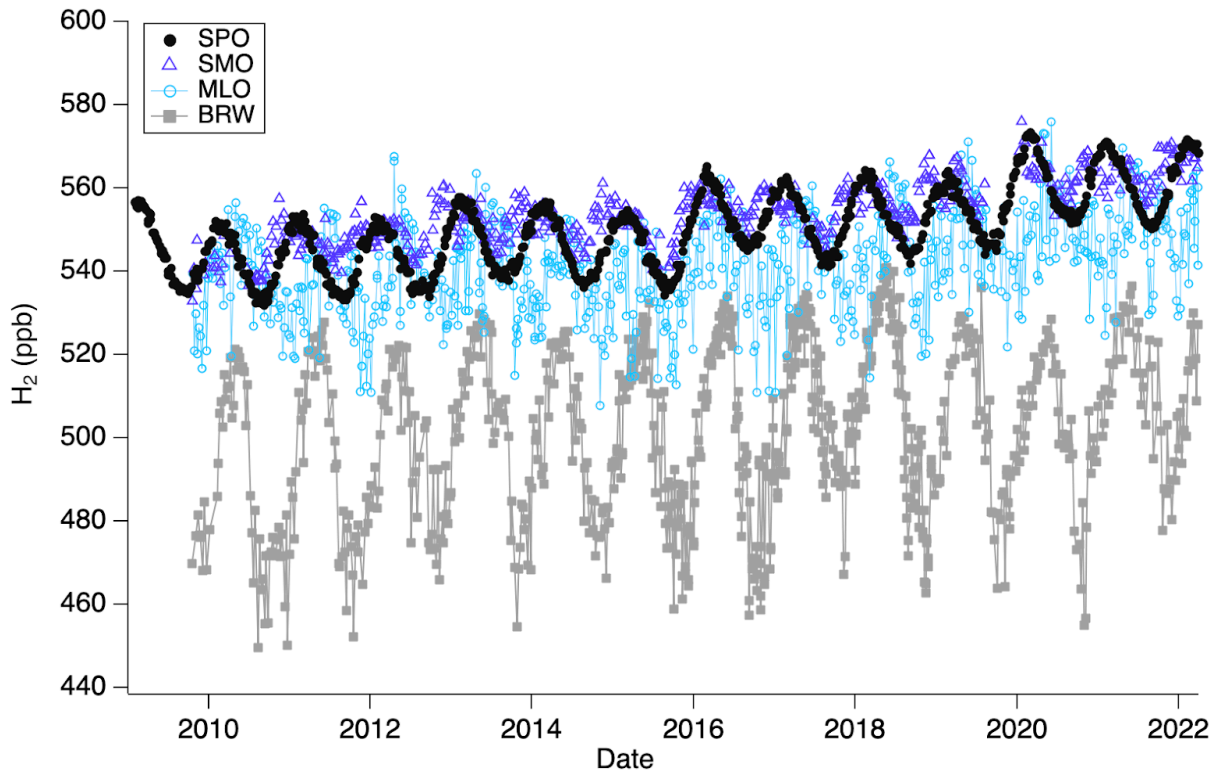


1251

1252 Figure 10. H₂ time series at the NOAA Baseline Atmospheric Observatories

1253

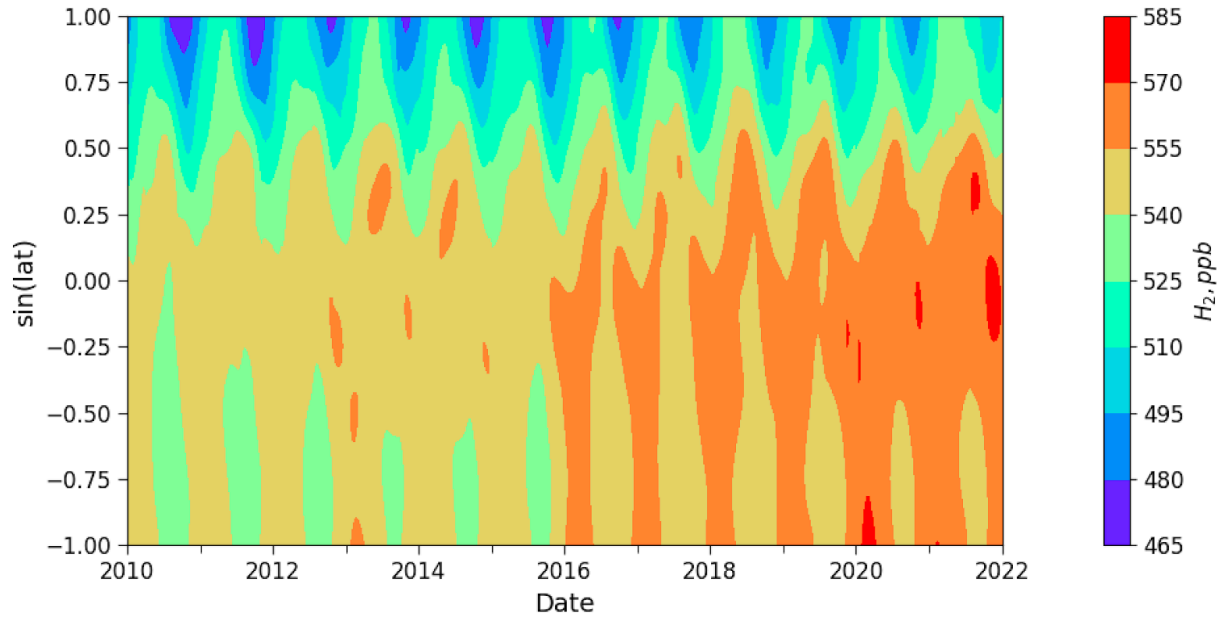
1254



1255

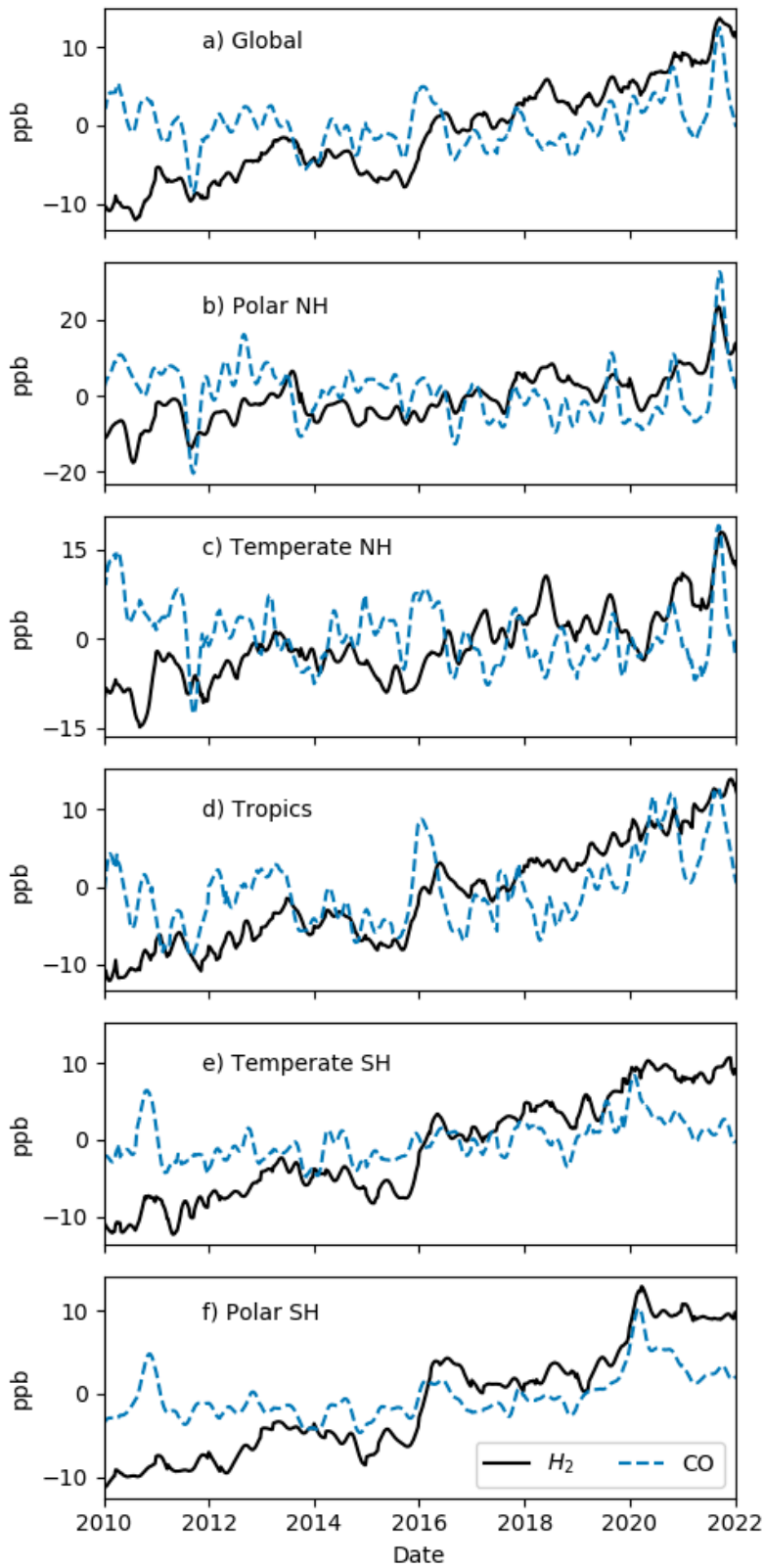
1256

1257 Figure 11: 2010-2021 marine boundary layer H₂ meridional gradient. Y-axis is the sine of latitude.
1258



1259
1260
1261
1262
1263

1264 Figure 12: 2010-2021 marine boundary layer global mean and zonal mean H₂ anomaly (black line) and
1265 CO anomaly (dashed blue line) time series.



1266